2011

An investigation into the paintbrush deposition technique for P3HT:PCBM based organic heterojunction solar cells

Aaron Lee Thoeming
Iowa State University

An investigation into the paintbrush deposition technique for P3HT:PCBM based organic heterojunction solar cells

by

Aaron Lee Thoeming

A thesis submitted to the graduate faculty

in partial fulfillment of the requirements for the degree of

MASTER OF SCIENCE

Major: Electrical Engineering

Program of Study Committee:

Sumit Chaudhary, Major Professor

Santosh Pandey

Nathan Neihart

Iowa State University

Ames, Iowa

2011

DEDICATION

I dedicate this academic work to my family. I will forever appreciate your support.

TABLE OF CONTENTS

LIST OF TABLES

LIST OF FIGURES

ACKNOWLEDGEMENTS

First and foremost, I would like to thank Dr. Chaudhary for taking me on as a student, providing funding, being a mentor, and being forgiving. I thank Dr. Pandey for teaching me about semiconductor physics and devices and for being on my committee. I also thank Dr. Neihart for being on my committee on such short notice. I thank Dr. Dalal for providing equipment, providing funding for my education through Iowa Power Fund, and for teaching me about semiconductor devices and physics. I thank Dr. Tuttle for providing references for me that have changed my life in positive ways. I thank Dr. Joe Shinar and Dr. Ruth Shinar for sharing research equipment and collaborating with me on my research studies

I thank Max Noack for teaching me practical issues concerning scientific research, for fixing broken equipment, and for being always kind. I thank Ben Curtin, Ryan Boesch, Alex Deutmeyer, Jason Jirak, Jeff Schmidt, Josh Riley, and Chris Ford for being excellent friends with me in my college years. I thank John Carr, Rakesh Mahadaevapuram, Kanwar Nalwa, Yuqing Chen, and Dan Putanm for being excellent research partners and friends. I thank Yuankun Cai, Min Cai, and Alexander Smith for working in collaboration on research.

I thank the Iowa State University Department of Electrical and Computer Engineering for providing me with teaching assistantships and for providing startup funding for my research group. I also acknowledge Iowa Power Fund for providing research equipment and funding for my education and research. I also would like to thank the Institute for Physical Research and Technology for providing me with a research assistantship.

ABSTRACT

Research in organic semiconductor materials and devices has increased dramatically in the last decade, particularly in the photovoltaics field. Organic based solar cells with record power conversion efficiencies of 8% to 9% have recently been reported, and future expectations for organic solar cell power conversion efficiencies are believed to approach 15%. Organic semiconductors hold interest due to their flexible mechanical properties and their ability to be solution processed. Processing techniques such as: spin coating, drop casting, roll painting, and ink jet printing can be readily used to deposit dissolved solutions of polymers and fullerenes to create organic solar cells. One novel, minimally researched solution processing technique for the deposition of polymer and fullerene solutions is paint brushing. Current research on paint-brushed solar cells has shown that solar cell efficiencies close to 5% can be obtained from active layer paint brushing on heated indium-tin-oxide covered glass substrates. In this study, organic solar cells are fabricated from P3HT and PCBM in chlorobenzene solution via paint brushing technique. Unlike previous studies, no heat treatment is applied to P3HT:PCBM active layers during or after device production. Paint-brushed devices are compared to spin-coated devices fabricated from the same P3HT:PCBM chlorobenzene solution in an effort to further investigate why paint-brushed solar cell devices perform better than non-annealed, spin-coated solar cell devices. Results from a full device characterization process including light current-voltage measurements, dark current-voltage measurements, active layer absorbance measurements, and external quantum efficiency measurements for both paint-brushed and spin-coated devices will be shown and discussed. Atomic Force Microscopy is used to provide active layer thickness data and film morphology information for both paint-brushed and spin-coated devices. Practical issues concerning using the paint-brush technique for organic solar cell fabrication are also covered.

CHAPTER 1. OVERVIEW

1.1 Introduction

This chapter is meant to provide a very basic introduction to the field of organic photovoltaics with a heavy emphasis on organic conjugated polymer/fullerene solar cell devices. In this chapter, the materials involved in fabricating organic conjugated polymer/fullerene solar cells will be described in brief. The currently used device architectures in organic conjugated polymer/fullerene solar cells will also be described to provide a background for the discussion of the fabricated devices detailed throughout this academic work. The unique fabrication methods involved in processing organic conjugated polymer/fullerene solar cells will also be covered to illustrate the possibilities of organic photovoltaics. Finally, an overview of previous research on the paint brush deposition technique for fabricating organic conjugated polymer/fullerene solar cells, a deposition technique central to the research presented in this academic work, will be presented. A further aim of this chapter, in general, is to provide both a historical and state-of-the-art context of this fascinating, rapidly emerging field of study in renewable energy science.

1.2 Organic Electronic Materials

This section briefly covers the materials utilized in organic photovoltaic devices. Both semiconducting polymers and fullerene molecules will be described from a physical standpoint. The functions of both polymer and fullerenes within organic photovoltaic devices will be explained. Photonic and electronic properties of semiconducting polymers will be discussed. Exciton formation and conduction within polymer molecules, in particular, will also be discussed. Specific examples of materials currently being used in organic photovoltaics will be presented.

1.2.1 Conjugated Polymers

Conjugated polymers are compounds comprised of alternating single and double bonds. In conjugated polymers, one p-orbital overlaps another p-orbital across a sigma bond along the conjugated polymer's backbone. This p-orbital overlap is a result of the sp^2 hybridization that occurs at the carbon centers in conjugated systems. The sp^2 hybridization that occurs in conjugated polymers allows for weakly bound delocalized π-electrons to be shared along the carbon centers in a conjugated system. In polymer-based photovoltaics, the delocalized π-electrons can be excited by photons into an anti-bonding state resulting in excitons. Through a charge transfer process, which will be discussed in detail later, photogenerated excitons within semiconducting polymers are broken up, allowing for the electrons and holes to be collected as current in a polymer based organic solar cell device. Conjugated polymers have energy band gaps that typically range between 1.9eV to 3eV and higher [1]. Unlike inorganic semiconductors with valence and conduction bands, semiconducting polymers have corresponding energy levels called the highest-occupied-molecular-orbital (HOMO) level and the lowest-unoccupied-molecular-orbital (LUMO) level that define the energy band gap of a semiconducting polymer. Exciton diffusion lengths within semiconducting polymers are on the order of 10nm [2, 3]. The low diffusion lengths of excitons are due to the low dielectric constants for conjugated semiconducting polymers, which typically range between two and four [4]. Figure 1.1 shows the polymer notation of poly(3-hexylthiophene) (P3HT), a widely used semiconducting polymer in organic photovoltaic research.

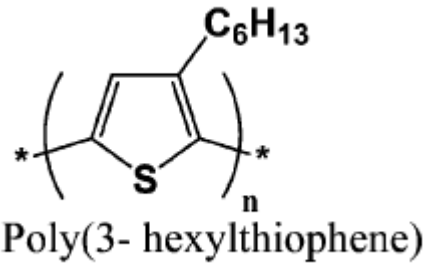

Figure 1.1 The Polymer Notation of Poly(3-hexylthiophene) [1]

1.2.2 Fullerenes

In 1985, Kroto et al. reported the discovery of the organic molecule, C_{60}, which is also known as a "buckminsterfullerene" [5]. This discovery led to a Nobel Prize in Chemistry for Kroto et al. in 1996. Figure 1.2 shows a picture of the molecular form of a buckminsterfullerene, C_{60}. As can be seen in Figure 1.2, C_{60} has the shape of a truncated icosahedron, which is the same shape as a soccer ball. Obviously, buckminsterfullerene and its shortened derivative, fullerene, are named after Buckminster Fuller, the inventor of the geodesic dome, which has the same shape as C_{60}. In 1992, Sariciftci et al. discovered electron transfer from excitons in a conducting polymer to a fullerene molecules [6]. That discovery would ultimately lead to the organic heterojunction solar cell device, which is the state of the art in organic photovoltaics today. In organic photovoltaics, fullerene molecules are utilized to break up photoinduced excitons generated in semiconducting polymers through a charge transfer process. The soluble fullerene derivative molecule [6,6]-Phenyl C_{61} butyric acid methyl ester (PCBM) is used instead of C_{60} because of its enhanced solubility in organic solvents [7]. Figure 1.2 shows the molecular notation of C_{60} and PCBM.

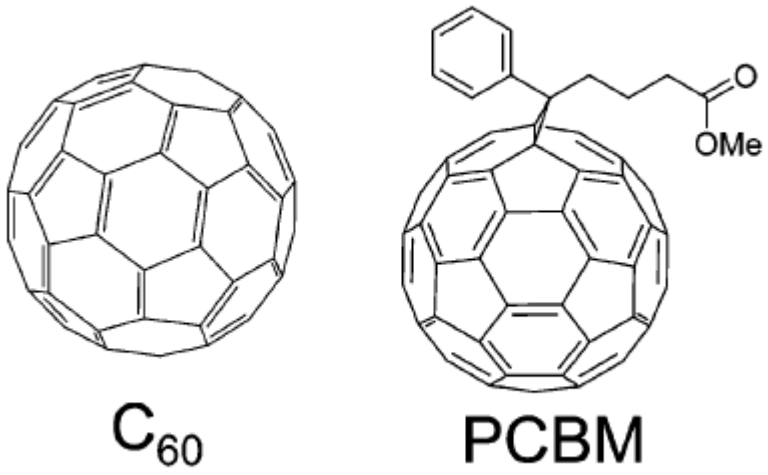

Figure 1.2 The Molecular Notation of C_{60} and PCBM [1]

1.3 Organic Photovoltaic Device Architectures

This section covers the various device architectures utilized in the study of organic photovoltaic devices. This section is not meant to be a comprehensive review of the device architectures of organic photovoltaic devices. A basic description of the different device architectures along with a discussion of the merits and weaknesses of each of the device architectures will be included in this section. Historical reports on organic solar cell device architectures and state of the art reports on organic solar cell device architectures will be discussed to provide both a historical background and a review of the present state of the field of organic solar cell research.

1.3.1 Single Layer Diode Device Architecture

The simplest of all organic polymer-based solar cell architectures has to be the single layer diode device architecture, also known as the metal-insulator-metal device architecture. In the single layer diode device architecture, two metal layers with asymmetric work functions sandwich an organic conjugated polymer layer. Figure 1.3 shows an energy band diagram for the single layer diode device architecture. As can be seen in Figure 1.3, the asymmetry between the work functions for the two metal anode and cathode layers provides the built-in electric field that separates excitons into separate electron and hole charge carriers when the solar cell is illuminated with solar energy, at least in theory. Due to the asymmetry of work functions between the anode and cathode metal layers, this device architecture displays rectifying characteristics with forward bias currents being magnitudes larger than reverse bias currents when evaluated at relatively low voltages [8].

Unfortunately, this architecture makes for better polymer-based organic light-emitting-diodes than for polymer-based organic solar cells. In this device architecture, under forward bias conditions, holes from the higher work function metal will be injected into the conjugated polymer film layer. Likewise, electrons from the lower work function metal will be injected into the conjugated polymer layer. Under forward bias, the electric field in the device for this device architecture reverses from its short-circuit orientation as seen in Figure 1.3, sweeping injected carriers towards the metal electrodes to be extracted as electrical current. The recombination

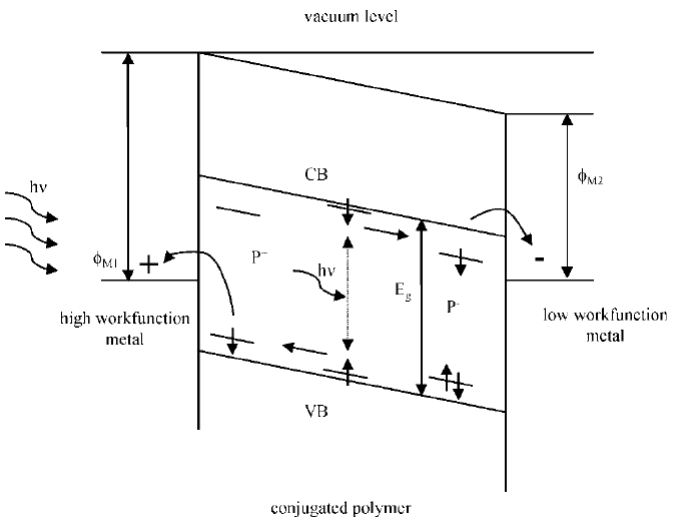

Figure 1.3 Single Layer Diode Energy Band Diagram [8]

of injected carriers under forward bias conditions provides for the electroluminescence required for LED operation. The photon energies emitted from a device with this architecture will be equal to the band gap between the HOMO and LUMO levels of the conjugated polymer layer. The first polymer-based organic light-emitting-diodes were designed with a nearly identical architecture by Partridge [9, 10, 11, 12]. Partridge utilized polyvinylcarbazole (PVCz) films in order to create blue light emitting polymer-based organic LED devices [11]. Partridge's devices slightly differed from the metal-insulator-metal architecture described here, by including a necessary positive charge injecting PVCz film reacted with antimony pentachloride ($SbCl_5$) [11]. Organic polymer-based light-emitting diodes that truly utilized the single layer diode architecture were first introduced in the early 1990's by research groups from Cambridge University and the University of California at Santa Barbara [13, 14].

Under short circuit conditions, a device utilizing the single layer diode architecture operates as a solar cell. Under reverse-bias conditions, the same device will operate as a photodetector. Unfortunately, this device architecture provides for poor solar cells and poor photodetectors. While the device is reverse biased, the built-in electric field due to the asymmetry between the metal electrode layers in the device is enhanced by the applied voltage. As the photodetector is illuminated with light, photons are absorbed, and excitons are generated. If the

electric field in the conjugated polymer layers is strong enough, then the electrons and holes comprising the excitons will disassociate and be swept towards the metal electrodes. However, photodetector devices created with the single layer diode architecture exhibit low power conversion efficiencies and low external quantum efficiencies, both being prerequisites for photodetection operation [15]. While operating as a solar cell, a device with this architecture will rely completely on the built-in electric field across the conjugated polymer layer to disassociate generated excitons. Unfortunately, the typical metal electrodes used in such devices, such as indium tin oxide and aluminum, do not provide a large enough built-in electric field capable of disassociating generated excitons. Typical dielectric constants for conjugated polymers range from two to four, making the coulombic attraction between the charge carries too strong to be overcome by the built-in electric filed of the device [4]. In these devices, current usually is extracted from excitons that are generated near contacts, where the excitons may disassociate through electron or hole transfer from the polymer and exciton to the corresponding metal electrode. Typical diffusion lengths of excitons generated in conjugated polymers are on the order of 10nm, which is incredibly small [2, 3]. With such low exciton diffusion lengths, any charges to be collected out of a device with the single layer diode architecture must come from excitons generated near the metal electrode layers. Solar cells made with this device architecture have power conversion efficiencies less than 0.1% and are no logner studied by research groups or companies [4].

1.3.2 Bilayer Heterojunction Device Architecture

The next evolution in organic polymer-based solar cell device architecture is the bilayer heterojunction device architecture, which is also known as the planar heterojunction device architecture. As described above, the main issue limiting the single layer diode device architecture was disassociating generated excitons. The bilayer device architecture overcomes this issue by including acceptor and donor layers in its architecture. The bilayer device architecture is comprised of two metal electrode layers with asymmetrical work functions, which provide a built-in electric field, sandwiching an electron donor layer and an electron acceptor layer in intimate contact. The intimate contact between the electron donor layer and the electron ac-

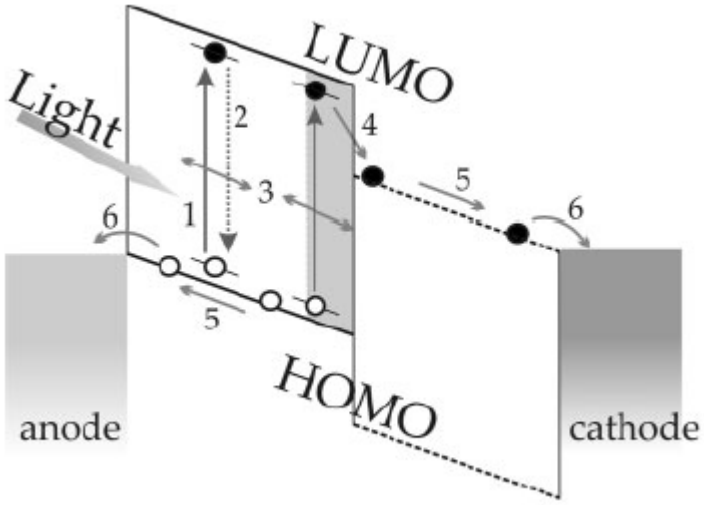

Figure 1.4 Bilayer Heterojunction Energy Band Diagram [4]

ceptor layer is the reason this device architecture is referred as a heterojunction, as opposed to homojunctions such as silicon p-n junctions. Figure 1.4 shows an energy band diagram for the bilayer heterojunction device architecture. The material comprising the electron donor layer has a smaller electron affinity, and the material comprising the electron acceptor layer has a larger electron affinity. This difference in electron affinities provides an energetically favorable interface for transferring the electrons from the generated excitons from the donor layer to the acceptor layer of the device. However, charge transfer between donor and acceptor layers in the bilayer heterojunction architecture does not guarantee the creation of free charge carriers. Once charge transfer between the electron donor layer and electron acceptor layer is complete, the electron and hole from the disassociated exciton are still coulombically attracted to each other and form what is known as a charge-transfer exciton, also known as geminate pair [16]. Free charge generation from charge-transfer excitons is aided by a built-in electric field in the device [16]. However, Mihailetchi et al. found that close to 60% of charge-transfer excitons in a PPV:PCBM donor acceptor system actually separate to produce free charge carries, showing that charge-transtfer exciton disassociaton can be a major loss mechanism in organic polymer based solar cells [17].

In 1986, Tang reported the first organic bilayer heterojunction solar cell, considered a

landmark moment organic photovoltaics [18]. In creating the first organic bilayer heterojunction solar cell, Tang was the first to introduce the heterojunction concept to the field of organic photovoltaics. Tang's bilayer heterojunction device utilized copper phthalcyanine (CuPc) and a perylene tetracarboxylic derivative as electron donor and electron acceptor small molecule layers. In fact, Tang's bilayer device was the first to exhibit exciton disassociation by charge transfer between electron acceptor layers and electron donor layers, a defining property for organic heterojunction devices. Tang's device achieved a power conversion efficiency of 1% under AM2 solar spectral irradiance, which is much higher than efficiencies reported from devices utilizing the single layer diode architecture. Tang's discovery of excitonic disassociation by means of charge tansfer bwtween electron donor layers and electron acceptor layers has heavily influenced the progress of organic photovoltaics. The operation of all current organic-based solar cells is based on the concept of exciton disassociation by means of charge transfer between electron donor and acceptor layers in hetrojunction device architectures.

Initially, bilayer heterojunction organic solar cell devices were made of thermally evaporated layers of organic small molecules[18]. With the discovery of photoinduced electron transfer from a semiconducting polymer to a buckminsterfullerene reported in 1992 by Sariciftci et al., bilayer heterojunction devices started to be comprised of spin-coated polymer electron donor layers and thermally evaporated C_{60} fullerene electron acceptor layers [6, 19, 20]. Research has also been reported on bilayer heterojunction solar cells incorporating polymer electron donor and acceptor layers [21, 22]. The invention of $PC_{61}BM$, a soluble derivative of C_{60}, has lead to fully solution processed polymer:fullerene bilayer heterojunction devices[7, 23]. In the case of polymer/polymer bilayer heterojunction devices and polymer/$PC_{61}BM$ bilayer heterojunction devices, care must be exercised in using orthogonal solvents for solution processing so that the spin coating of one organic layer does not dissolve the previously deposited layer. The current record in power conversion efficiency for a bilayer heterjunctoin solar cell, as reported by Lee et al., is 3.8% [23]. The major limitation with the bilayer heterojunction architeture is the low diffusion length of generated excitons. In order for free charges to be created, excitons must be generated within their diffusion length to the bilayer interfacial junction so that they may be disassociated and contribute to the photogenerated current. However, Lee et al. have

found that $PC_{61}BM$ actually diffuses into and mixes with the polymer layer when forming a bilayer heterjunction solar cell through solution processing [23]. This intermixing at the interface probably allows for more excitons to be harvested into free charge carriers, incressing the overall efficienes of such "bilayer" devices. These results suggest that bilayer heterojunction devices may provide higher efficiencies if further studied.

1.3.3 Bulk Heterojunction Device Architecture

Though recent research shows promise for bilayer heterojunction devices, the state of the art in organic solar cell architectures is the bulk heterojunction architecture, which is also known as the dispersive heterjunction architecture. The single layer diode architecture has proven to be ineffective as a solar cell do limitations in disassociating generated excitons. As mentioned previously, exciton disassociation in single layer diode devices occurs only at the electrodes because the built-in electric field provided by the metal electrode layers is not enough to overcome the coulombic attraction between the charge carriers in excitons. Due to low exciton diffusion lengths on the order of 10nm in conjugated polymers, only photons absorbed near the metal electrodes in single layer diode devices will contribute to photogenerated current [2, 3]. Bilayer heterojunction devices were developed to overcome the issue of exciton disassociation by incorporating a heterojunction interface that is energetically favorable for charge transfer and exciton disassociation between organic electron and donor acceptor layers. Unfortunately, bilayer devices require excitons to be generated within an exciton diffusion length of the heterojunction interface or metal electrodes in order to contribute to generated photocurrent. In both the single layer diode architecture and bilayer heterjunction device architecture exciton diffusion limits the overall power conversion efficiency in devices. To overcome the exciton diffusion limits of the previous architectures, the bulk heterojuncton device architecture was invented.

The device structure of a bulk heterojunction organic solar cell comprises an organic active layer composed of an intermixed network of electron acceptor molecules and electron donor molecules sandwiched between metal electrode layers of asymmetric work function, with one of those metal electrode layers usually being a transparent conductive oxide coated on a glass slide.

The intermixed active layer for such devices is created by either thermally evaporating electron donor and electron acceptor molecules at the same time or, more commonly, by solution processing via spin coating a solution containing electron donor and electron acceptor molecules. Due to the intermixing of electron donor and electron acceptor molecules throughout the active layer, heterojunction interfaces exist throughout the volume of the active layer. With heterojunction interfaces throughout the volume of the active layer in a bulk heterojunction device, a greater probability that generated excitons will be disassociated into free charge carriers that can contribute to the photogenerated current exists as compared to devices with the single layer diode architecture and bilayer heterjunction architecture. The reason generated excitons are more likely to be disassociated into free carriers in bulk heterojunction devices than in other device architectures is that a greater heterojunction surface area exists in bulk heterojunction devices due to the electron donor and electron accepting molecules being intermixed throughout the volume of such devices. Along with the greater heterojunction interface surface area in bulk heterojunction devices, the intermixing of electron donor and electron acceptor molecules throughout the volume of the active layer allows excitons generated throughout the active layer to be disassociated into free charges, which is in stark contrast to the other organic solar cell device architectures that require excitons to be generated within an exciton's diffusion length of metal electrode layers or a rigidly defined heterojunction interface in the bilayer heterojunction case. Figure 1.5 shows the energy band diagram of a bulk heterjunction solar cell, detailing the energy gap overlap between the electron acceptor molecules and electron donor molecules due to the intermixing of both types of molecules in this type of devices.

The first solar cell devices to utilize the bulk heterojunction device architecture were first reported by Yu et al. in 1995 [24]. Yu et al. showed that devices made by spin coating solutions of intermixed polymer and fullerene molecules could lead to forming solar cell devices with the bulk heterojunction device architecture. These initial devices were made by using mixed polymer/fullerene solutions of the semiconducting conjugated polymer, MEH-PPV, and the fullerenes: C_{60}, [5,6]PCBM, and [6,6]PCBM. In these devices, and in virtually all polymer/fullerene based organic solar cells, the polymer acts as an electron donor, and the fullerene acts as the electron acceptor. C_{60} is not very soluble in organic solvents, and its derivatives,

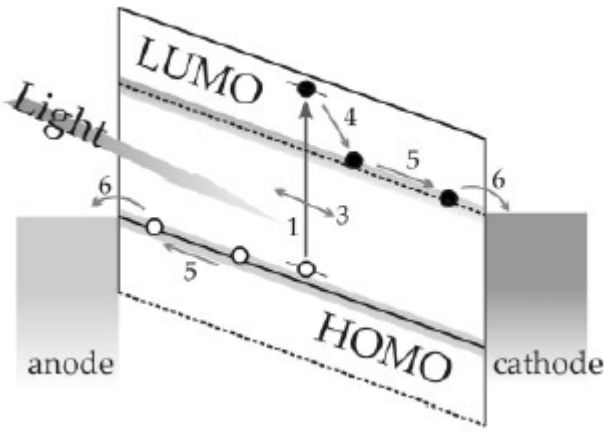

Figure 1.5 Bulk Heterojunction Energy Band Diagram [4]

[5,6]PCBM and [6,6]PCBM, were synthesized by Hummelen et al. for the purposes of expanding the possibilities of solution processing in organic photovoltaics [24, 7]. Yu et al. were the first to use the [6,6]PCBM C_{60} derivative in polymer/fullerene solar cells. PCBM is currently widely used in polymer/fullerene based organic solar cells as an electron acceptor.

The first truly power efficient organic bulk heterojunction devices with 2.5% power conversion efficiencies were reported by Shaheen et al. in 2001 [25]. Shaheen et al. created bulk heterjunction devices using the conjugated polymer, MDMO-PPV, and the fullerene derivative, $PC_{61}BM$. In creating their devices, Shaheen et al. utilized toluene and chlorobenzene to see the effects that different organic solvents may have on the morphology of the bulk heterjunction active layer. Shaheen et al. found that devices spin-coated with cholorbenzene solutions performed much better than the devices spin-coated using toluene solutions. Upon further investigation using atomic force microscopy technology, Shaheen et al. determined that spin-coated films produced from chlorobenzene solutions resulted in films with less material phase segregation. Figure 1.6 shows the atomic force microscopy topographical images of spin-coated films from the study. With less phase segregation of the conjugated polymer and fullerene molecules in the chlorobenzene films, Shaheen et al. found that the chlorobenzene based devices performed better than the toluene based devices due to better exciton disassociation into free carriers due to the better intermixing of the conjugated polymer and fullerene molecules

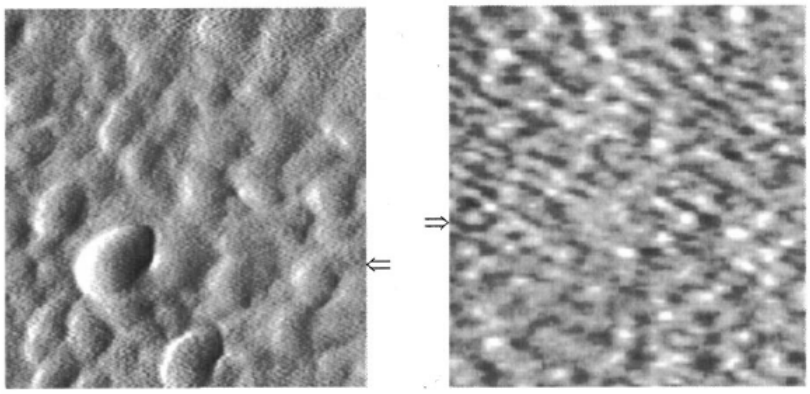

Figure 1.6 Atomic Force Microscopy Topographical Images of MDMO-PPV:PCBM Films (Toluene Right, Chlorobenzene Left) [25]

in the chlorbenzene based devices. Shaheen et al. speculated that the better intermixing of conjugated polymer and fullerene molecules is a result of $PC_{61}BM$ being much more soluble in chlorobenzene than in toluene. This study by Shaheen et al. showed that morphology of the active layer is crtically important for solar cell device performane in bulk heterojunction organic solar cells. Furthermore, the study showed that organic solvents have a direct impact on the morphology.

The next leap in power efficiency in organic bulk heterjunction solar cells came in 2005 from two research groups within the University of California system [26, 27]. Both groups utilized the conjugated polymer, P3HT, and the fullerene, $PC_{61}BM$ in making their devices; however, the two groups used different organic solvents for solution processing. Ma et al. of the University of California at Santa Barbara organic photovoltaics group fabricated P3HT/PCBM bulk heterojunction organic solar cell devices using chlorobenzene as the organic solvent [26] for solution processing. Ma et al. reported the effects of post production annealing on P3HT/PCBM bulk heterojunction solar cells fabricated via spin coating from chlorobenzene solutions. Through their research, Ma et al. found that performing post production thermal annealing, or heating after full device fabrication, resulted in highly efficient organic bulk heterojunction solar cells. By performing post production annealing at 150°C for 30 minutes, Ma et al. were able to achieve power conversion efficiencies of 5% for P3HT/PCBM organic bulk heterojunction solar cells fabricated from chlorobenzene solution. Ma et al. attributted the high power conversion

efficiencies achieved by these devices to the improved nano-scale morphology of the active layer upon annealing. The improved nano-scale morpholgy in the thermal annealing these devices provided better exciton disassociation and better charge transport due to the higher molecular crystalinity within the bulk heterojunction active layer. Ma et al. also found that post production annealling provides for better adhesion between the aluminum contact and the active layer in devices as compared to devices that are annealed prior to evaporating the top metal electrode. The better adhesion between the top metal electrode and the active layer in post production annealled devices was thought to aid in charge transfer from the active layer to the top metal electrode, decreasing the series resistance in such devices.

The second group mentioned above is based out of the University of California at Los Angeles. Li et al. of the organic photovoltaics group at the University of California at Los Angeles reported results for organic bulk heterojunction solar cell devices utilizing the conjugated polymer, P3HT, and the fullerene, PCBM [27]. Unlike the research group out of Santa Barbara, Li et al. used dichlorobenzene as the organic solvent for solution processing. The organic solar cell study conducted by Li et al. differed from the study conducted by the Santa Barbara group by focusing on the slow growth of the nano-morphology of the active layer in organic bulk heterojunction solar cell devices instead of focusing on the effects of thermal annealing on such devices. In their study, Li et al. controlled the solvent annealing of bulk heterojunction active layer films by controlling the film solidification rate of those films. Solvent annealing essentially refers to how the morphology of the active layer in spin-casted bulk heterjunction films settles as the solvent evaporates from the spin-casted films. To control the solvent annealing and morphology growth rates in bulk heterojunction active layer films, Li et al. used petri dishes to slow the solvent annealing time and morphology growth rate while using heat to speed up the solvent annealing time and morphology growth rate. Li et al. found that slowing the solvent annealing time and growth rate of organic bulk heterojunction films resulted in higher power conversion efficiency solar cell devices. The slower grown organic bulk heterjunction films exhibited higher hole mobilities and greater crystallinity within the bulk heterojunction film morphologies. By slowing the down the solvent annealing time and consequently slowing the growth of the bulk heterojunction film morphology, Li et al. were able to fabricate P3HT/PCBM based organic

bulk heterjunction solar cells from dichlorobenzene solution that achieved power conversion efficiencies close to 4.4%, which is on par with the devices created by the Santa Barbara organic photovoltaics research group.

As can be determined from the results of these previous studies, the morphology of active layer films in organic bulk heterojunction solar cell devices is of critical importance with regard to the output performance of such devices. Solution processing is an incredibly complex process with many variables to take into account. In the 2001 study conducted by by Shaheen et al., the experimental results suggest that the type of organic solvent used can affect the resulting morphology of active layer films in organic bulk heterojunction solar cells [25]. The Santa Barbara organic photovoltaics group showed that post production thermal annealing also affects the morphology of organic bulk heterojunction films [26]. Also, the Los Angeles organic photovoltaics research group found that slowing the solvent annealing, or film drying time, affected the morphology of bulk heterojunction films [27]. Other variables that might affect the morphology of bulk heterojunction films include: polymer and fullerene solution concentrations, solution deposition techniques, and the fabrication environment. A diagram of an ideal bulk heterojunction morphology is shown in Figure 1.7. As can be seen in Figure 1.7, an ideal morphology for an organic bulk heterjunction solar cell has interdigitated electron donor and electron acceptor phases that ideally are spaced within an exciton's diffusion length to ensure that all generated excitons are disassociated into free charge carriers. In an ideal organic bulk heterojunction morphology, a pure electron donor phase would completely cover the surface area of the hole collecting electrode to better conduct holes out of the electron donor phase. Likewise, a pure electron acceptor phase would completely cover the surface area of the electron collecting electrode to better conduct electrons out of the electron acceptor phase. Obviously, fabricating an organic bulk heterojunction solar cell with the film morphology illustrated in Figure 1.7 would be incredibly difficult.

Current research in bulk heterojunction solar cells is trending away from the use of the conjugated polymer, P3HT, as the the electron donor and towards the use of novel polymers tuned to have lower band gaps and lower HOMO levels. Brabec et al. determined in 2001 that the origin of open circuit voltage in organic bulk heterojunction is due to the difference

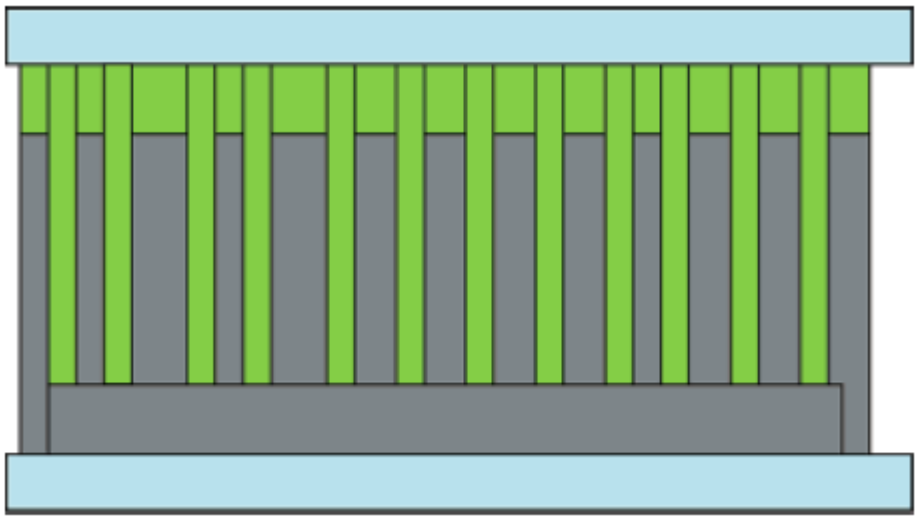

Figure 1.7 Ideal Morphology of a Bulk Heterjunction Solar Cell (Grey = Conjugated Polymer, Green = Fullerene) [1]

in energy between the HOMO level of the electron donor molecule and the LUMO level of the electron acceptor molecule [28]. Because the vast majority of organic bulk heterjunction solar cells utilize PCBM as the electron acceptor molecule, tuning the HOMO level of the polymer is usually the only option for increasing the open circuit voltage in organic bulk heterjunction solar cells. In 2009, Park et al. reported a then world record power conversion efficiencies of 6.1% for organic bulk heterojunction solar cells utilizing the polymer, PCDTBT, and the fullerene, $PC_{71}BM$ [29]. Park et al. found that by using the polymer, PCDTBT, as an electron donor molecule in organic bulk heterojunction solar cells, the open circuit voltage for the reported organic bulk heterojunction solar cells was relatively high at 0.88V due to the relatively low HOMO level of PCDTBT. Park et al. also utilized a titanium suboxide optical spacer in their solar cell device architecture to increase photon absorption in the bulk heterojunction active layer and to act as a barrier to holes near the electron collecting electrode, reducing charge carrier loss through recombination. Figure 1.8 shows a figure of the band diagram and device architecture for the devices Park et al. reported. Also in 2009, Chen et al. reported 6.77% efficient organic bulk heterojunction solar cell devices that utilized the low band gap polymer, PBDTTT, and the fullerene, $PC_{71}BM$ [30]. Chen et al. found that chemically

altering PBDTTT by adding electron withdrawing functional groups lowered the HOMO level of PBDTTT and, consequently, increased the open circuit voltages of their reported organic bulk heterjunction solar cell devices. By combining the effects of increased light absorptoin of a low bad gap polymer with the chemical tuning of the HOMO level of that polymer, Chen et al. were able to report devices that set a then world record in organic solar cell power conversion efficiency. Liang et al. have reported on the highest journal published power conversion efficiencies for organic bulk heterjunction solar cell devices [31]. Liang et al. have reported 7.4% power conversion efficiencies for organic bulk hererojunction solar cell devices utilizing the polymer, PTB7, and the fullerene, $PC_{71}BM$. Despite all the recent advances in power conversion efficiency for organic bulk heterjunction solar cells, there may still be more room to improve. Based on modeling and simulation studies, Koster et al. believe that the power conversion efficicency for organic polymer/fullerene based bulk heterojunction solar cells may approach 11% through tuning the band gap of polymers, tuning the LUMO levels of electron acceptor molecules, and developing morphologies that favor free carrier transport for both electrons and holes in order to avoid space charge effects [32]. Although polymer/fullerene based bulk heterjunction devices are widely researched, small molecule based organic bulk heterjunction solar cells and polymer/polymer based organic bulk heterojunction devices also have been researched [33, 34, 35].

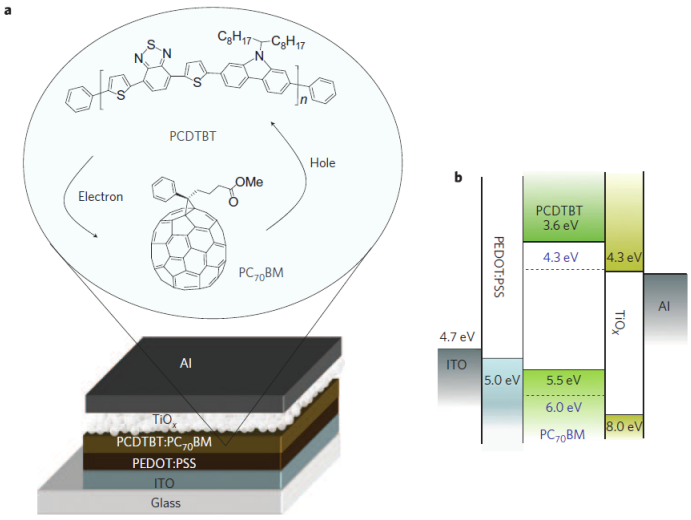

Figure 1.8 State of the Art Bulk Heterjunction Solar Cell [29]

1.3.4 Tandem Organic Solar Cells

In 1961, William Shockley and Hans J. Queisser theoretically derived the maximum power conversion efficiency of a p-n homojunction solar cell [36]. From their theoretical analysis, Shockley and Queisser were able to calculate maximum theoretical power conversion efficiencies for p-n homojunction solar cells with differing material band gap energies. Figure 1.9 shows a plot for the theoretically determined maximum power conversion efficiencies for p-n homojunction solar cells of differing energy band gaps. As can be seen in figure 1.9, Shockley and Queisser determined that the maximum power conversion efficiency obtainable from a p-n homojunction solar cell made of a material with an energy band gap of 1.1eV, like silicon, is around 30%. Shockley and Queisser determined that the maximum theoretcial efficiencies of p-n homojunction solar cells are greately determined by the energy bad gap of the material in p-n homojunction solar cells. Photons with energies lower than the energy band gap of the semiconducting material comprising the p-n homojunction solar cell will not be absorbed, limiting the efficieny of such devices. However, photons with enegies greater than the band gap of the semiconductor material comprising the p-n homojunction solar cell are absorbed as "hot" electrons. Unfortunately, some of the energy absorbed from photons with energies greater then the band gap of the semiconducting material of solar cell devices is lost as heat due to the thermalization of the solar cell from "hot" electrons.

Multi-junction solar cell devices, also known as tandem solar cells, have been created using materials of differing energy band gaps to better absorb photons and to reduce thermalization losses due to "hot" electrons. In 1980, Alexis De Vos reported theoretically determined maximum power conversion efficiencies for tandem solar cells [37]. For unconcentrated cells, Vos determined that two-cell and three-cell unconcentrated tandem solar cells would exhibit 42% and 49% maximum power conversion efficiencies under illumination of one sun of irraddiance respectively. Vos also found that two-cell and three-cell concentrated tandem solar cells would have maximum power conversion efficiencies increase to 55% and 63%respectively. These theoretcial maximum efficiencies are much higher than the 30% that Shockley and Queisser predicted for single p-n homojunctions solar cell devices due to the fact that mulitjunction devices

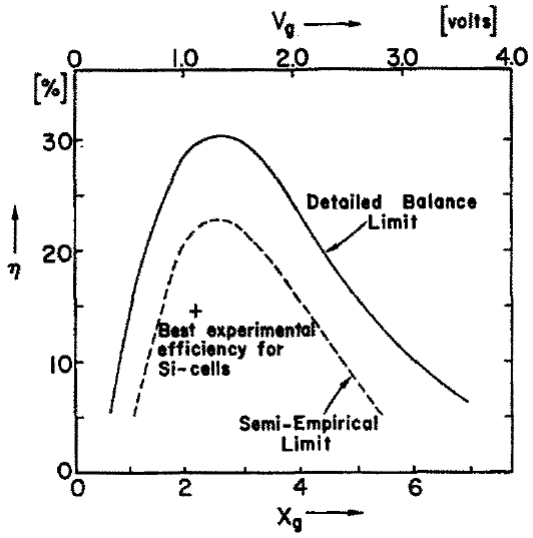

Figure 1.9 Shockley-Queisser Limit of p-n Homojunction Solar Cells [36]

make better use of absorbed photon energy. Vos went further with theoretcial predictions on tandem solar cell maximum power conversion efficiencies and found that a tandem cell with an inifinitie number of solar cells would have a maximum power conversion efficiency of 68% for unconcentrated sunlight and 86% for concentrated sunlight. Typically, inorganic tandem solar cell devices are comprised of the so called III–V semiconducting materials, including gallium and indium. However the rarity of some III–V materials and the complicated epitaxial growth processing involved with III–V materials make inorganic tandem solar cells expensive.

Organic based tandem solar cell device architectures have been studied since 1990 in an effort to increase the power conversion efficiencies of organic solar cell devices [38]. Organic tandem solar cells come in a few different varieties. The earliest tandem cells were composed of two cells that were fabricated by evaporating small molecules for the organic solar cell active layers [38]. The next in evolution of organic tandem solar cells are "hybrid" tandem solar cells, not to be confused with inorganic/organic hybrid solar cells. "Hybrid" organic tandem solar cells are composed of two solar cells with one solar cell fabricated by thermally evaporating small molecules and the other fabricated via solution processing [38]. Finally, organic tandem solar cells have been fabricated with active layers completely formed by solution processing [38]. Figure 1.10 shows the band diagram of an arbitrary organic tandem solar cell comprised of two

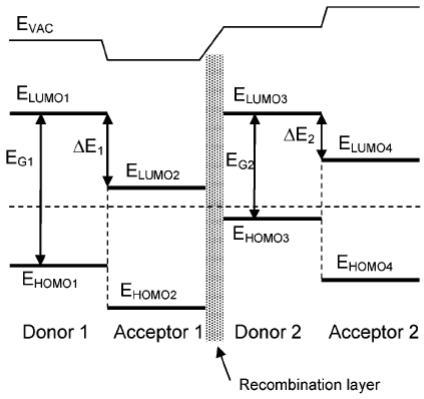

Figure 1.10 Energy Band Diagram for an Arbitrary Organic Tandem Solar Cell []

organic solar cells. As can be seen in Figure 1.10, an intermediate layer is required in order to connect the solar cells in an organic tandem solar cell device in either a series configuration or parallel configuration. The intermediate layer in an organic tandem solar cell must act as recombination layer for holes injected from the electron donor of one solar cell and electrons injected from the electron acceptor in the other solar cell in a two-cell device in order to avoid space charge effects. Also, the intermediate layer in an organic tandem solar cell must at least be somewhat transparent in order to allow light to be absorbed in the other solar cells that comprise the device.

In 2007, Kim et al. reported on a highly efficient organic tandem solar cell devices that were nearly completely solution processed [39]. In the devices reported on by Kim, et al., only the top metal electrode and the bottom ITO electrode were deposited without solution processing. Kim et al. were able to achieve power conversion efficiencies of 6.5% for their nearly completely solution processed organic tandem solar cells. The reported solar cells utilized two organic bulk heterojunction solar cells with the following material configuratoins: PCDTBT/PC_{61}BM and P3HT/PC_{71}BM. Figure 1.11 shows a diagram and a transmission electron microscopy image of the architecture of the tandem solar cell that Kim et at. reported. For the interfacial intermediate layer connecting the two bulk heterojunction solar cells in series, Kim et al. used a transparent titanium suboxide optical spacer. The titanium suboxide optical spacer was deposited via sol gel chemistry. The titanium suboxide layer is a novel addition to the organic

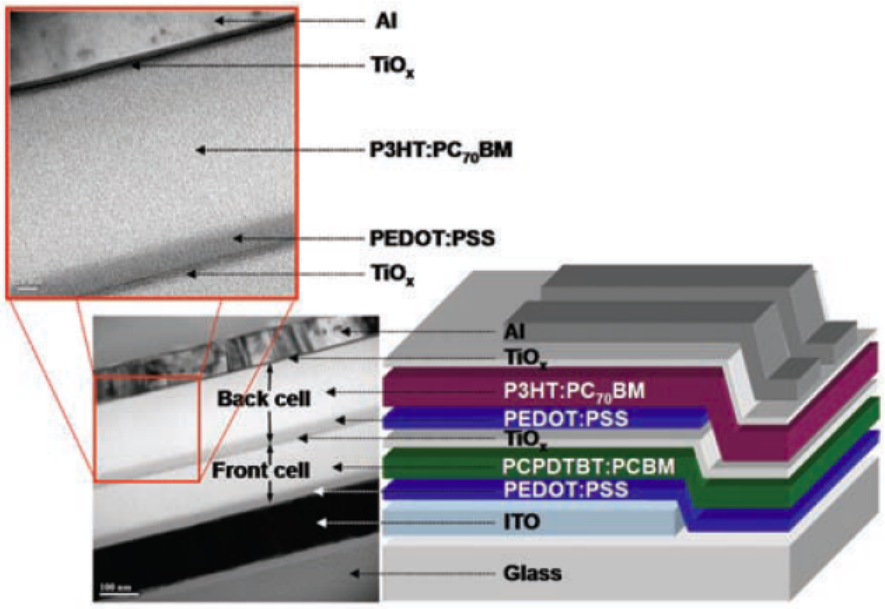

Figure 1.11 Device Architecture for a Solution Processed Organic Tandem Solar Cell [39]

tandem solar cell device architecture created by Kim et al. because it serves many purposes that allow for an efficient nearly completely solution processed organic tandem solar cell. The titanium suboxide layer serves as protection to the first solar cell from the fabrication of the second solar cell in the organic tandem solar cell. The titanium suboxide optical spacer also acts as an electron collecting layer for the first solar cell and a hole blocking layer for the second solar cell in the organic tandem solar cell, allowing the middle PEDOT:PSS layer to act as a recombination layer. Finally, the titanium suboxide intermediate layer acts as an optical spacer in redistributing the light intensity into the P3HT/PC_{71}BM solar cell. Figure 1.12 shows the energy band diagram for the organic tandem solar cell that Kim et al. reported. The most interesting design element of the devices reported by Kim et al. is that having the solar cell with the lower energy band gap polymer in front of the solar cell with the higher energy band gap makes for a more efficient organic tandem solar cell. That design element is counterintuitive because thermalization loses due to the generation of "hot" electrons from photons with energies much greater than the absorbing material's energy band gap are regarded as the main reason for reduced power conversion efficiencies in solar cell devices.

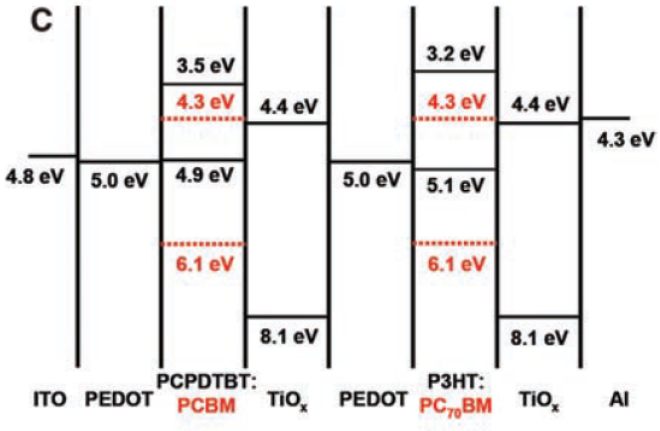

Figure 1.12 Energy Band Diagram for a Solution Processed Organic Tandem Solar Cell [39]

The nearly completely solution processed organic tandem solar cells reported by Kim et al. are incredibly novel; however, the device power conversion efficiencies for organic devices are expected to increase. Independently, Kotlarski et al. and Dennler et al. have theoretically predicted maximum power conversion efficiencies of 14%–15% for organic bulk heterojunction two-cell tandem solar cells [40, 41]. If these predictions hold, then the potential for improvement of the power conversion efficiencies of organic tandem solar cells certinaly exists. Considering that theoretically predicted values for the maximum power conversion efficiency for single-cell organic bulk heterojunction solar cells is reported to be close to 11%, organic tandem solar cells may end up being required in order to make organic solar cells efficient enough to be cost effective [32].

1.4 Organic Electronic Fabrication Techniques

A major point of interest in the field of organic electronics is the fabrication of organic electronic devices. Inorganic semiconductor processing techniques usually involve complicated, expensive processes that require high temperatures and high vacuums. Examples of complicated and expensive processes involved in inorganic semiconductor device fabrication include molecular beam epitaxy, chemical vapor deposition, ion beam implantation for doping, wet and dry oxidation in high temperature furnaces, sputtering, and ultraviolet photolithography to name

a few. Initially, studies in organic electronic devices dealt with small organic molecules that are sometimes referred to as pigments. Fabrication involving small organic molecules usually involved thermally evaporating small organic molecules to form thin semiconducting layers. The first organic heterojunction solar cell was made by thermally evaporating organic electron accepting and electron donating small molecule layers [18]. Eventually, the fabrication of organic heterojunction solar cells evolved to include solution processable semiconducting conjugated polymers as electron donor molecules along with organic small molecule electron acceptor materials, such as C_{60}, that still required thermal evaporation for film deposition. With the advent of the solution processable fullerene derivatives, $PC_{61}BM$ and $PC_{71}BM$, full solution processing of organic heterjunction solar cells began to be realized [7].

1.4.1 Spin Coating

The great promise of organic electronics lies in the solution processability of the conjugated polymers and fullerenes used in organic electronic devices. Solution processing allows for many unique, cost effective fabrication methods. The most popular method for depositing the organic thin films for research purposes, by far, is spin coating. Spin coating is a simple and compact fabrication technique that allows for depositing uniform organic films via solution processing. Figure 1.13 shows an illustration of the spin coating fabrication technique. As can bee seen in Figure 1.13, a solution containing organic semiconducting materials is dropped onto a flat substrate situated on what historically is called a "wafer chuck," due to the widespread use of spin coating in silicon wafer processing in the semiconductor industry. The flat substrate is held down to the "wafer chuck" by a vacuum provided by a mechanical pump. A motor spins the "wafer chuck" and attached substrate with solution, leaving a thin, uniform organic film. Unfortunately, spin coating is not a technique that produces large area devices or is compatible with roll-to-roll processing, a requirement for making organic solar cell devices cost effective. Spin coating is also wasteful of materials, as most of the solution deposited on the substrate prior to spinning is spun off the substrate during the spinning process. Despite its disadvantages, spin coating is a very useful technique for organic solar cell research in both academia and industry.

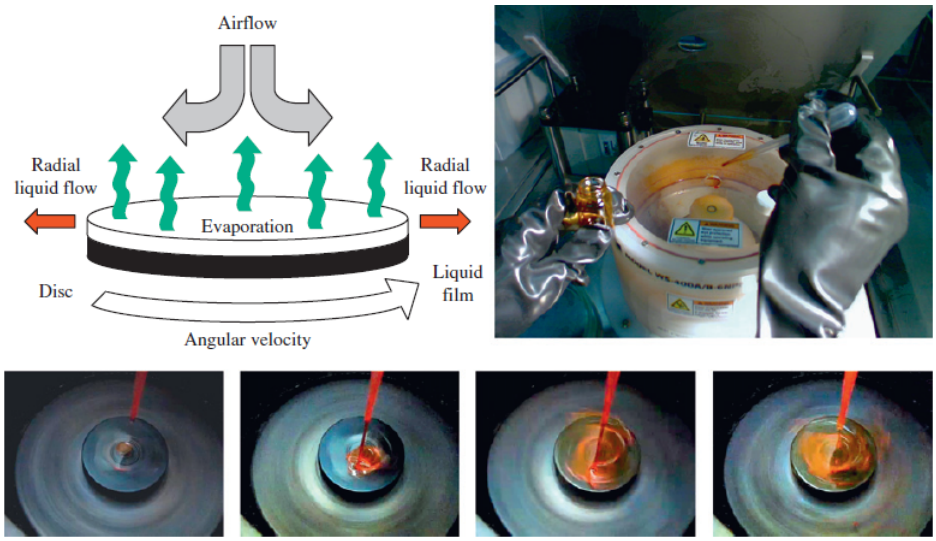

Figure 1.13 An Illustration of the Spin Coating Fabrication Technique [42]

1.4.2 Drop Casting

The simplest solution processing method for fabricating organic solar cell devices is the drop casting method. In the drop casting method, a solution containing organic semiconducting materials is dropped in a controlled fashion on an, ideally, horizontal substrate. Figure 1.14 shows an illustration of the drop casting technique along with the possible results of the drop casting technique. As can be seen in Figure 1.14, drop casting can produce variable results from nice, homogeneous organic films (lower left) to poor organic films that show "picture-framing" (upper right) and precipitation effects during drying (lower right). In order to get nice, homogeneous organic films from drop casting, appropriately strong solvents must be used to ensure that precipitation does not occur during the drying process of the drop casted films. Drop casting is a technique that allows for creating thick organic films; however, there is minimal control over the thicknesses of resulting organic films, which is a major disadvantage of this technique.

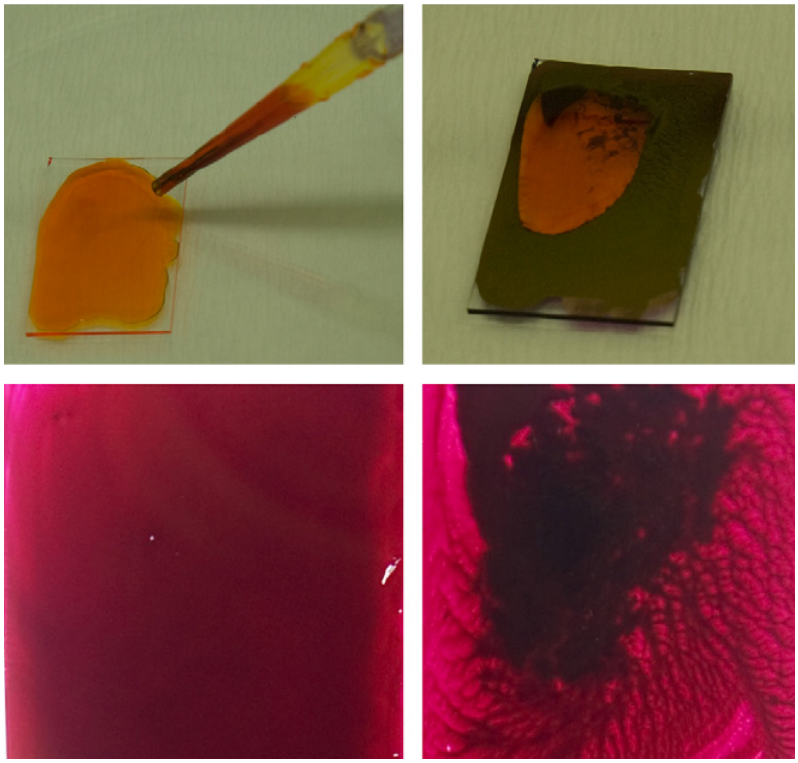

Figure 1.14 An Illustration and Results of the Drop Casting Fabrication Technique [42]

1.4.3 Dip Casting

Dip casting is another simple solution processing technique for fabricating organic electronic devices. As the name of the technique suggests, thin organic films are deposited on substrates by dipping substrates into solutions containing organic semiconducting materials. Dip casting is mostly used on non-conventional substrates such as fibers. Figure 1.15 shows an illustration of a novel fiber-based organic bulk heterjunction solar cell device fabricated by Lee et al. by using an advanced form of dip casting technique. In order to create the device depicted in Figure 1.15, Lee et al. drew a stainless steel wire through vertically aligned set of consecutive coating cups, each cup filled consecutively with solutions containing materials for the electron transport layer, the bulk heterojunction active layer, and the hole transport layer [43]. Each of the coating cups contained a hole with a diameter slightly larger than the diameter of the metal wire to allow the metal wire to pass through with an intact freshly coated layer. Ovens lie between each of the coating cups in order to dry the fresh coatings from the last coating cup. For the secondary

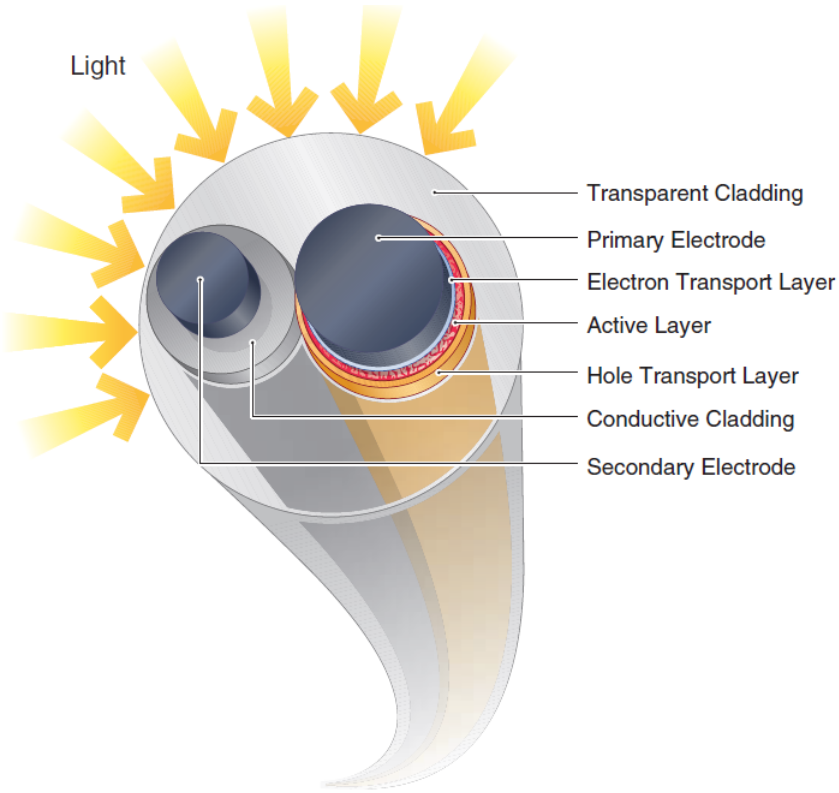

Figure 1.15 A Diagram of a Fiber-based Organic Solar Cell [43]

electrode, Lee et al. coated a second stainless steel wire with silver paste using the same coating method used for the primary electrode wire. The second silver coated stainless steel wire acts as a secondary electrode to extract holes from the primary electrode wire. To complete the circuit in the fiber-based solar cell device, Lee et al. wrapped the secondary electrode wire around the primary electrode wire. Lee et al. used a titanium suboxide layer for the electron transport layer and PEDOT:PSS for the hole transport layer. The active layer in these fiber-based organic solar cells was composed of the conjugated polymer, P3HT, and the fullerene, $PC_{61}BM$. Lee et al. were able to achieve power conversion efficiencies of around 3.27% for the fiber based organic solar cells they reported. Dip casting is not a popular solution processing technique in the field of organic electronics; however, for specialized circumstances like in the sub-field of fiber-based organic electronics, dip casting can be a very useful fabrication technique.

1.4.4 Doctor Blading

Doctor blading is a solution deposition technique that is not widely reported on in the organic electronics research community. The doctor blading technique involves spreading a solution across a flat substrate using a sharp blade fixed a small distance above the substrate. During the doctor blading operation, a solution containing organic semiconducting materials is deposited in front of the sharp blade while the sharp blade is moved linearly along the substrate. Figure 1.16 shows pictures of an Erichsen Coatmaster 509MC-I Doctor Blading System while idle and in operation. Typical operating spacing distances between the sharp blade and substrate range from 10 µm to 500 µm, depending on the desired film thickness [42]. Equation 1.1 gives the resulting film thickness from using the doctor blading technique [42]. In Equation 1.1, the variables: g, c, and ρ correspond to the gap between the sharp blade and flat substrate, the concentration of the organic solutes in the solution, and the density of the organic solutes from the solution in the final dry film, respectively.

$$d = \frac{1}{2}\left(g\frac{c}{\rho}\right) \tag{1.1}$$

Doctor blading has some advantages and disadvantages when compared to other solution processing techniques. One advantage of the doctor blading technique is that it can be modified to work in a roll-to-roll system in a configuration called "knife-over-edge." However, for small scale laboratory purposes, spin coating is preferred over the doctor blading technique. The doctor blading technique is much slower than spin coating, typically operating at speeds of 1mm to 100mm per second [42]. Due to the slow deposition speeds of the doctor blading technique, organic material agglomeration in the final films can be a problem. Another advantage of doctor blading technique is that it can be calibrated to waste very little material during the deposition process. If calibrated correctly, the doctor blading technique can minimize material loses to less than 5% [42].

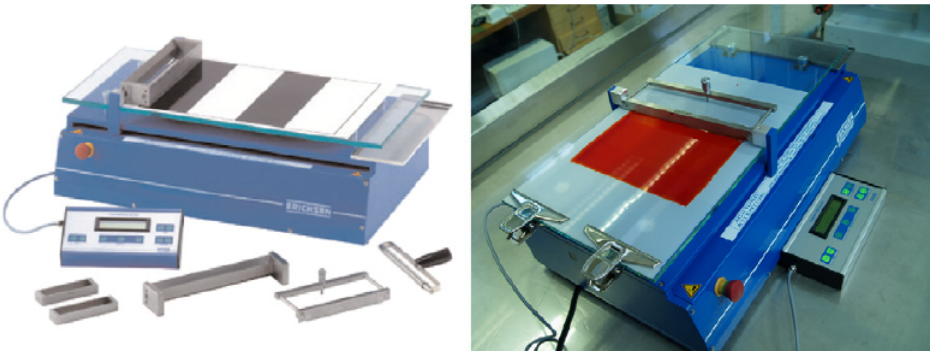

Figure 1.16 A Picture of an Erichsen Coatmaster 509MC-I Doctor Blading System [42]

1.4.5 Screen Printing

Screen printing is an ancient technique used for stenciling patterns onto substrates. In screen printing, a fine woven mesh is held under tension by a frame while ink is pressed through the mesh using what is called a squeegee onto a desired substrate. To create patterns, parts of the woven mesh are emulsified to block ink from being pushed through the woven mesh in those areas. In order for the patterning to work in screen printing, the emulsification of the woven mesh must be impervious to the ink used for printing. Figure 1.17 shows a basic illustration of the screen printing process. Screen printing requires using a solution of high viscosity, which is a limiting factor in solution processing organic semiconducting materials [42]. Although screen printing is naturally suitable for batch processing, screen printing is a technique that is adaptable to roll-to-roll processing, which is a requirement for producing cost effective organic solar cell devices.

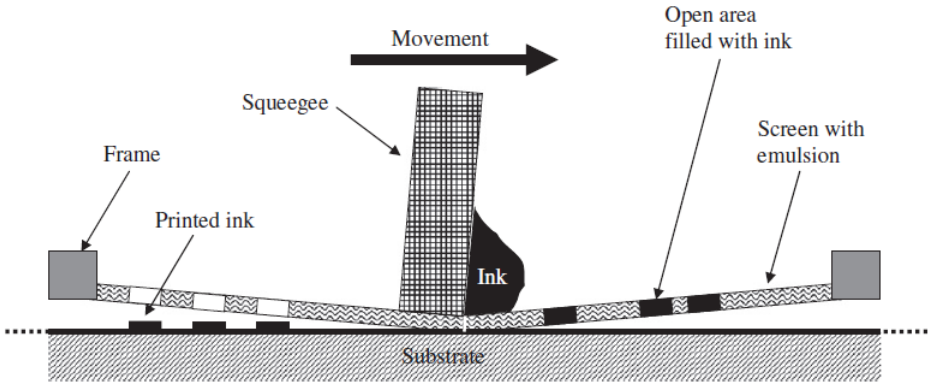

Figure 1.17 A Basic Illustration of the Screen Printing Process [42]

1.4.6 Ink Jet Printing

Ink jet printing is a solution deposition technique that developed from the office printing industry. Ink jet printing is an attractive solution processing technique due to its capability of relatively high resolutions of 300dpi to 1200dpi [42]. In ink jet printing, droplets are formed by pressures produced either by applied heat or by piezoelectric mechanical stress. A digital signal is used to control the rate at which droplets are formed. After being formed, the droplets are charged by charging electrodes and accelerated towards the target substrate by an electric field. Figure 1.18, shows a basic illustration of the ink jet printing process [42]. One advantage of ink jet printing over other methods of printing is that the desired printed image is stored digitally, making a physical mask outlining the desired image unnecessary. Ink jet printing is a solution processing technique that is compatible with roll-to-roll processing, making it an attractive technique for the organic electronics industry.

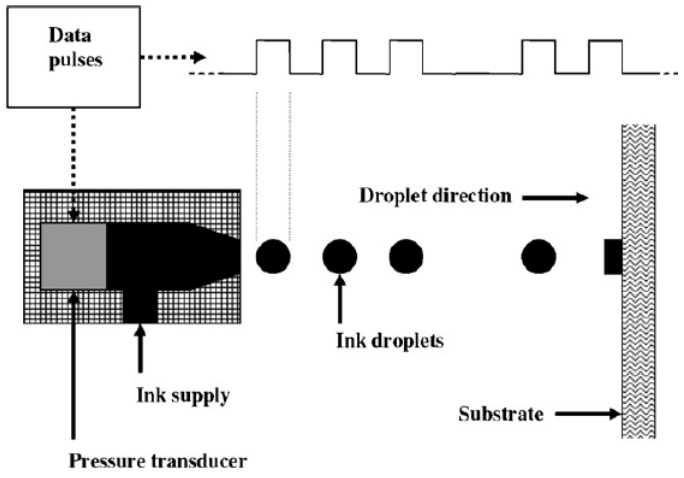

Figure 1.18 A Basic Illustration of the Ink Jet Printing Process [42]

1.4.7 Roller Painting

Roller painting is a novel solution processing technique recently reported on in research literature. In 2010, Jung et al. were the first to report on organic bulk heterojunction solar cell devices fabricated by utilizing the roller painting solution processing technique [44]. Jung et al. fabricated organic bulk heterojunction solar cell devices by roller painting a combined so-

lution of the conjugated polymer, P3HT, and the fullerene, $PC_{61}BM$, in dichlorobenzene upon glass slides coated with indium-tin-oxide and a buffer layer of PEDOT:PSS. For comparative purposes, Jung et al. also fabricated organic solar cell devices by spin coating the active layers, using the same solutions and parameters utilized for the roller painted devices. Jung et al. found that roller painted devices exhibited power conversion efficiencies of around 2.4% for non-annealed devices and 4.6% for thermally annealed devices. On the other hand, Jung et al. found that the spin-coated organic solar cell devices performed worse with power conversion efficiencies of around 1.9% for non-annealed devices and 3.9% for thermally annealed devices. Further measurements such as x-ray diffraction measurements, absorbance measurements, mobilty meaurements, and transmission electron microscope imaging lead Jung et al. to conclude that the organic solar cell devices fabricated by roller painting contained active layers that featured more crystalline P3HT fibers and more $PC_{61}BM$ nanocrystals. Jung et al. theorized that a combination of the shear stresses applied to the active layer solution during the roller painting procedure and the slower drying times of the resulting films from the roller painting technique.

Expanding upon their results with roller painting on smaller substrates, Jung et al. fabricated organic solar cell devices with relatively large $5cm^2$ active layers on indium-tin-oxide coated glass substrates. In addition to fabricating on larger substrates, Jung et al. included the additive, octanedi-1,8-thiol, to the solution containing the organic semiconducting materials. The solution additive, octanedi-1,8-thiol, was used to help phase separation in the resulting active layer bulk heterjunction films, negating the need for post-fabrication thermal annealing. Jung et al. found that organic solar cells with active layers of $5cm^2$ could achieve power conversion efficiencies of 2.7% when fabriacted using the roller painting technique and 0.8% when fabricated by spin coating without any post-fabrication thermal annealing. The farily decent power conversion efficiency exhibited by the large area roller painted organic solar cells fabricated by Jung et al. is an exciting development, showing that power efficient, large area organic solar cells can be faricated without the need for annealing. Roller painting is a solution processing technique that is highly compatible with roll-to-roll processing. The combination of large area fabrication, annealing free fabricatoin, simplicity of fabrication, and compatibility with

roll-to-roll processing could make roller painting a highly desirable technique for fabricating organic solar cell devices in industry.

1.4.8 Roll-to-Roll Processing

Roll-to-roll processing is the main focus of fabrication within the organic photovoltaics industry. The promise of organic photovoltaics lies in the cost effectiveness in solution processing large area solar cell devices. Organic materials also have flexible mechanical properties which make them unique amongst semiconductor materials. Roll-to-roll processing takes advantage of both the benefits of solution processing and the benefits of mechanical flexibility of organic materials used for organic electronic devices to create organic electronic devices on a large scale at a fast rate, reducing the overall cost of such devices. Roll-to-roll processing is also very flexible with regard to compatibility of fabrication techniques utilized in the processing of organic electronic devices. Of the fabrication techniques widely used in fabricating organic electronic devices today, spin coating is probably the only fabrication technique not compatible with roll-to-roll processing. Figure 1.19 illustrates a narrow sample of fabrication techniques compatible with roll-to-roll processing.

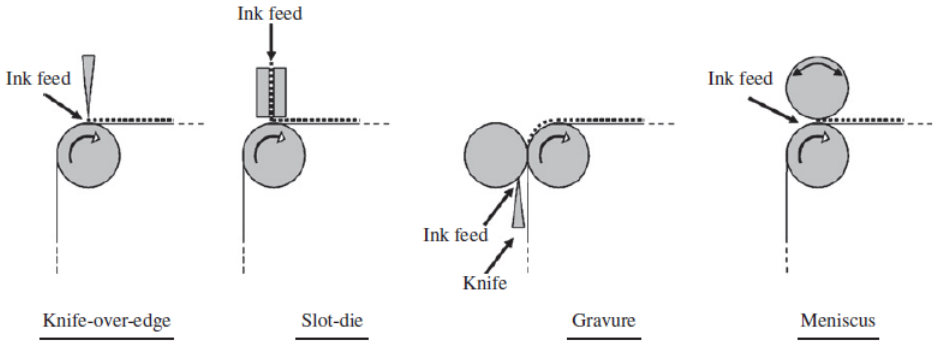

Figure 1.19 Roll-to-Roll Processing Fabrication Techniques [42]

1.5 Paintbrush Deposition Technique

One novel, minimally researched fabrication technique for creating organic solar cell devices not mentioned in the previous section is the paintbrush deposition technique, which is the main

focus of this academic work. In 2007, Kim et al. of the Heeger Center of Advanced Materials at the Gwangju Institute of Science and Technology were the first to report on organic bulk heterojunction solar cell devices comprised of the conjugated polymer, P3HT, and the fullerene, $PC_{61}BM$ fabricated using the paintbrush deposition technique [45]. Kim et al. reported organic bulk heterojunction solar cell devices with power conversion efficiencies close to 5.4% fabricated by utiliyzing the paintbrush deposition technique to apply the active layer of the devices. To create their devices, Kim et al. used a paintbrush equipped with nylon fibrils to deposit the bulk heterojunction active layer from a solution of P3HT and PCBM dissolved in chlorobenzene onto a PEDOT:PSS layer spin-coated upon an indium-tin-oxide coated glass slide. Figure 1.20 shows an artistic interpretation of paintbrush deposition technique for depositing the organic active layers for organic bulk heterojunction solar cell devics. During the fabrication of the organic bulk heterojunction solar cell devices, Kim et al. heated the PEDOT:PSS and indium-tin-oxide covered glass slide substrate at the same time as applying the organic active layer using the paintbrush deposition technique. Kim et al. found, through experimentation, that heating the indium-tin-oxide and PEDOT:PSS coated glass substrates at 50^oC while paint-brushing the active layer produced the best organic solar cell devices. The resulting devices fabricated by Kim et al. showed better performance compared to completely spin-coated organic bulk heterojunction solar cells, with higher fill factors, short circuit currents, and open-circuit voltages. Utilizing x-ray diffraction measurements and absorbance measurements, Kim et al. were able to determine that organic bulk heterojunction solar cell devices fabricated using the paintbrush deposition technique had better ordering of the polymer chains than the organic bulk heterjunction solar cell devices fabricated completely by spin coating. The better ordering of the polymer chains in the paint-brushed solar cell devices was hypotheszied by Kim et al. to be a result of shear stress applied by the paintbrush during active layer film deposition. Kim et al. concluded that the better ordering of the polymer chains in the paint-brushed organic solar cell devices was the reason for the better performance over the fully spin-coated organic solar cell devices.

In 2010, Kim et al., from the same group at the Heeger Center of Advanced Materials at the Gwangju Institute of Science and Technology that reported the first organic solar devices

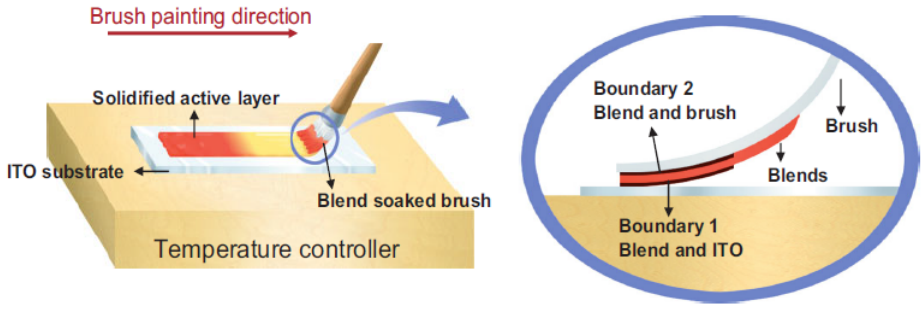

Figure 1.20 Illustration of the Paintbrush Deposition Technique for Organic Bulk Heterojunction Solar Cells [45]

partially fabricated utilizing the paintbrush deposition technique, reported on organic bulk heterojunction solar cells in which the active layer and the PEDOT:PSS buffer layer were both deposited via the paintbrush deposition technique [46]. Kim et al. were able to report organic bulk heterjunction solar cell devices with both the P3HT/PCBM active layer and the PEDOT:PSS buffer layer deposited via the paintbrush deposition technique that achieved power conversion efficiencies close to 3.6%. Unlike the previous study on the paintbrush deposition technique, Kim et al. utilized dichlorobenzene as the organic solvent to disolve the P3HT polymer molecules and the $PC_{61}BM$ fullerene molecules. Due to the change in organic solvent from chlorobenzene to dichlorobenzene, Kim et al. had to increase the temperature during the paintbrush solution deposition step from 50^{o}c to 110^{o}C due to the higher boiling point of dichlorobenzene. In this study, Kim et al. found that the organic solar cell devices fabricated utilizing the paintbrush deposition technique perfomed better than the organic solar cell devices fabricated by spin coating both the bulk heterojunction active layer and the PEDOT:PSS buffer layer. Kim et al. utilized x-ray diffraction measurements, atomic force microscopy, and mobility measurements to determine that organic solar cell devices fabricated utilizing the paintbrush deposition technique had better ordering of the polymer chains within the active layer than the organic solar cell devices fabricated by spin coating.

The studies conducted by Kim et al. of the Heeger Center of Advanced Materials at the Gwangju Institute of Science and Technology are the first of their kind regarding the use of paint brushing as a fabrication technique in solution processing organic solar cell devices.

However, the studies conducted by Kim et al. have a large flaw. In both studies, Kim et al. claimed that no pre-fabrication or post-fabrication heat treatment was applied to the organic solar cell devices fabricated by paint brushing, which is not true. Organic solar cell devices fabricated by paint-brushing were heated during the paint brushing step in both studies. In the first study, the paint-brushed organic solar cell devices were heated at 50^{o}C during the paint brushing of the active layer step. In the second study, paint-brushed organic solar cell devices were heated at 110^{o}C during the paint brushing of the active layer step due to the switch from using chlorobenzene to dichlorobenzene as the organic solvent. Thermal annealing, a heat treatment, has previously been shown to improve the performance of organic bulk heterojunction solar cell devices by favorably altering the nano-scale morphology of the bulk heterojunction active layer and by increasing the ordering of the polymer chains within the bulk heterojunction active layer [26]. Unfortunately, the studies conducted by Kim et al. do not decouple the heat treatment from the paintbrush deposition technique, making it impossible to determine whether the use of the paintbrush deposition technique is solely the reason for increased device performance of paint-brushed organic solar cell devices over spin-coated organic solar cell devices. The aim of the rest of this academic work is to report on the fabrication, characterization, and analysis of paint-brushed organic solar cell devices without any heat treatment applied to the active layer of the devices during or after device fabrication.

CHAPTER 2. METHODS and PROCEDURES

2.1 Device Fabrication

This section of Chapter 2 details the fabrication processes utilized to produce both spin-coated and paint-brushed organic bulk heterojunction solar cell devices. Each step of the fabrication process, from substrate cleaning to the deposition of the top metal electrode, will be discussed in detail. Practical issues pertaining to the fabrication techniques utilized in fabricating the organic bulk heterojunction solar cell device will also be discussed. Equipment used during the fabricating steps will be explained to provide the reader a "real world" perspective on organic solar cell processing.

2.1.1 Fabrication Environment

All inorganic semiconductor devices require manufacturing processes that include specific fabrication environments and conditions for each fabricating step within the device manufacturing process. For instance, environments containing high-level vacuums are required for thin-film deposition of inorganic semiconductor materials and metal films. Inorganic semiconductor materials used in semiconductor devices, such as silicon wafers, are often required to be handled in clean room environments to avoid unwanted doping of the semiconductor materials. Clean room environments also help prevent dust contamination that leads to inorganic semiconductor device destruction due to physical damage to the planar layers involved in inorganic semiconductor devices. As with inorganic semiconductor devices, organic semiconductor devices require fabrication specialized fabrication environments during fabrication as well. At the research level, organic semiconductor device active layers are usually deposited in an argon environment contained within a glovebox. The argon environment within the glovebox helps

to prevent oxygen and water vapor exposure to organic semiconductor devices as the organic semiconductor active layers are being deposited. Depositing organic semiconductor active layers within a glovebox environment also provides the added advantage of limited dust particle exposure to organic semiconductor devices under fabrication.

Multiple fabrication environments were utilized during the manufacturing process of the organic bulk heterojunction solar cell devices in this study. Initially, the indium-tin-oxide coated glass slide substrates of the organic bulk heterojunction solar cell devices in this study were prepared under normal ambient atmosphere conditions up to, but not including, the deposition of the organic semiconductor active layer. For depositing the organic semiconductor active layers of the organic bulk heterojunction solar cell devices, the device substrates were transferred into a glovebox containing an argon atmosphere. Once the organic semiconductor active layers were deposited upon the devices, the devices were exposed to a high-level vacuum during the thermal evaporation of the top metal electrode of the devices. The metal deposition process and equipment will be described in detail in Section 2.1.5.

The glovebox used for the fabrication of the bulk heterojunction devices in this study is a four-compartment MBRAUN MB 20G glovebox equipped with two small antechambers and one large antechamber for transferring items in and out of the glovebox. The MBRAUN glovebox is equipped with a circulation system that includes oxygen and water vapor sensors, and a copper catalyst purifier for purifying the argon environment held by the glovebox. A solvent trap including a MANN filter and activated carbon, a very porous material, is also placed within the circulation system to protect the copper catalyst purifier from particle and chemical contamination. The MBRAUN glovebox is periodically sourced argon by external argon gas cylinders. Periodically, the copper catalyst purifier needs to be regenerated by removing oxides from the carbon formed over time through usage. An argon cylinder with 4% by volume hydrogen is used to regenerate the copper catalyst purifier by having the hydrogen react with oxides on the copper catalyst, with the resulting water vapor flushed out of the system. An Edwards brand mechanical pump serves the MBRAUN glovebox system by providing vacuums necessary for the transfer of items through the antechambers and for controlling the pressure of the argon environment within the glovebox.

2.1.2 Substrate Cleaning

Organic electronic devices are not remotely subject to the rigorous clean fabrication environment standards as those required for the inorganic semiconductor industry. In the inorganic semiconducting industry, and in particular the semiconductor chip manufacturing industry, high standards exist for the fabrication environment for inorganic semiconductor devices. Contaminates from the ambient air atmosphere can "dope" the structural lattice of semiconductors, significantly altering the electrical properties of the semiconductor materials and subsequently fabricated semiconductor devices. Contaminants from human beings, such as oils from the skin, also play a role in "doping" semiconductor materials. Dust contaminates from the ambient air atmosphere can structurally damage inorganic semiconductor devices with feature sizes approaching 32nm and less. Due to the stringent cleanliness requirements for fabrication, inorganic semiconductor device fabrication requires the use of cleanrooms and high level vacuums.

Fortunately, organic electronic materials do not share the same stringent clean environment requirements for which inorganic semiconductor materials are subject. Nevertheless, organic electronics processing does require a certain amount of care with regards to clean processing methods. In particular, clean substrates are of importance for fabricating organic electronic devices. Indium-tin-oxide coated glass slides are widely used in organic electronics research, particularly in the photovoltaics branch of organic electronics, as a substrate for device fabrication. Any dirt or dust that exists on the indium-tin-oxide coated glass slide substrate can affect the solution processing involved in organic electronics fabrication. Typically, organic semiconducting layers are deposited upon a substrate via solution processing using techniques such spin-coating or any roll-to-roll processing compatible solution deposition techniques. Any dust or dirt upon the device substrates can impede solution flow during the solution processing, affecting the nano-morphology of the resulting deposited organic layers and, thus, affecting the performance of the resulting organic electronic devices. Dust and dirt on device substrates can also lead to "pin holes" in organic electronic devices, causing shorting in organic electronic devices.

In this study, indium-tin-oxide (ITO) coated glass slide device substrates are cleaned using cleaning solutions coupled with ultrasonic cleaning. ITO coated glass slides undergo a four-step solution cleaning process. Prior to cleaning the ITO coated glass slides, four solutions are created, with each solution corresponding to a step in the cleaning process. The four solutions are made up of the following mixtures of chemicals, respectively: 2-propanol and acetone, Alconox detergent in deionized water, methanol and ethanol, and, finally, deionized water. Each of the described cleaning solutions are placed in 50mL centrifuge tubes that are capable of holding three 1″ X 1″ ITO coated glass slides. The 2-propanol and acetone solution is measured to a 1:1 ratio by volume. Likewise, the methanol and ethanol solution is also measured to a 1:1 ratio by volume. During the device substrate cleaning process, ITO coated glass slides are placed in the 50mL centrifuge tubes containing the cleaning solutions and are subjected to ultrasonic cleaning by a Cole-Parmer 8891 Ultrasonic Cleaner. The ITO glass slides are perpendicularly stacked upon each other in the 50mL centrifuge tubes in order to ensure that the faces of the glass slides fully benefit from the solution enhanced ultrasonic cleaning. For ultrasonic cleaning, the 50mL centrifuge tubes containing the cleaning solution and glass slides are held by a clamp and partially submerged in the water-filled basin of the ultrasonic cleaner. The ITO coated glass slides are ultrasonic cleaned for ten minutes in the 2-propanol and acetone solution, then for another ten minutes in the Alconox detergent solution, followed by ten more minutes in the methanol and ethanol solution, and, finally, 10 minutes in deionized water. The ITO coated glass slides are rinsed by agitated dipping in a beaker filled with fresh deionized water between transferring from one cleaning solution to another. After the solution aided ultrasonic cleaning, the ITO coated glass slides are dried off by using a blow gun connected to a pressurized gas cylinder containing nitrogen. Once dry, the ITO glass slides are placed in wafer boxes in preparation for the next step of the fabrication process, the deposition of the transparent conductive buffer layer.

2.1.3 Transparent Conductive Layer Deposition

After cleaning the ITO coated glass slide substrates by solution-assisted ultrasonic cleaning, the transparent conductive buffer layer was deposited via spin coating. The transparent con-

ductive buffer layer used in the organic bulk heterojunction solar cells in this study is Poly(3,4-ethylenedioxythiophene) poly(styrenesulfonate), henceforth referred to as PEDOT:PSS. Before spin coating the PEDOT:PSS solution upon the ITO coated glass slide substrates, the glass substrates undergo plasma cleaning to increase the wettability of the ITO surface of the glass substrates to ensure that a uniform PEDOT:PSS layer is formed during spin coating. An Harrick PDC-32G Plasma Cleaner is used to plasma clean the glass slide substrates with an air plasma for five minutes. Once the glass slide substrates have been plasma treated, the PEDOT:PSS solution is immediately spin-coated upon ITO surfaces of the glass substrates in a fume hood. A syringe with an attached Whatman 0.45μm hydrophilic PVDF filter is used to deposit the PEDOT:PSS solution to the ITO surfaces of the glass substrates prior to spin-coating. Filtered PEDOT:PSS solutions were spin coated on ITO coated glass slide substrates at 3000RPM for 60s. An Headway Research Spin Coating system was utilized for spin coating the PEDOT:PSS layers upon the glass slide substrates. A Franklin Electric mechanical vacuum pump was used to provide the vacuum necessary to hold the glass slides to the wafer chuck while spin coating. After the spin coating of the PEDOT:PSS layer on the glass slide substrates, the glass slide substrates were annealed on a Fisher Scientific Isotemp Hotplate for 5 minutes at 120^{o}C to boil off the water solvent used in the PEDOT:PSS solution. A PEDOT:PSS transparent conducting layer is required for organic bulk heterojunction solar cell devices to prevent the surface roughness of the sputtered ITO layer on the glass slide substrates from creating "pin-holes" in the organic active layers of organic solar cell devices.

2.1.4 Active Layer Deposition

Once the PEDOT:PSS active layer has been established upon the ITO surfaces of the glass slide substrate, the organic active layer of the organic bulk heterojunction solar cell devices is deposited upon the PEDOT:PSS layers. In this study, the active layers of organic bulk heterojunction solar cell devices were fabricated by spin coating and paint brushing. Initially, a solution comprising semiconducting polymer donor molecules and fullerene acceptor molecules is created within an argon glovebox environment and stirred for at least twelve hours before being deposited upon substrates to form organic bulk heterojunction active layers for organic

solar cell devices. In this study, Poly(3-hexylthiophene), henceforth referred to as P3HT, and [6,6]-Phenyl C_{61} butyric acid methyl ester, henceforth referred to as PCBM, were dissolved by chlorobenzene to form a 1:1 weight ratio solution. This solution was stirred for twelve hours at 45^oC on a hot plate the day before the active layer deposition for the organic solar cells in this study. P3HT serves as the electron donor material within the bulk heterojunction active layer of the organic solar cell devices fabricated for this study. Likewise, PCBM serves as the electron acceptor material within the organic solar cell devices fabricated for this study.

Before depositing the organic bulk heterojunction active layers, the glass substrates with the deposited PEDOT:PSS layers were transferred into an argon atmosphere glovebox containing the solution for forming the organic active layers of the devices in this study. For the spin-coated devices, the organic solution mentioned previously was deposited onto the PEDOT:PSS covered ITO glass substrates by a syringe equipped with a Fisher 0.2μm PTFE hydrophobic filter. The spin-coated devices were spin-coated at 600RPM for 60s. After spin coating, the spin-coated organic solar cell devices were placed under a petri dish to dry, a practice known as "solvent annealing." The spin-coated devices, however, were virtually dry coming off the wafer chuck from the spin coater. For the paint-brushed devices, the organic active layer solution was filtered into small beaker using the same filter as for the spin-coated devices. A Royal branded white nylon fiber paintbrush was used to deposit the filtered organic solution onto the PEDOT:PSS ITO glass slide substrates. Only a single coating was used for creating the organic bulk heterojunction active layers for the paint-brushed devices. A nylon fiber paintbrush was used for fabricating the paint-brushed devices because chlorobenzene does not dissolve nylon. As with the spin-coated devices, the paint-brushed devices were solvent annealed under a petri after the deposition of the organic active layers. Unlike the spin-coated devices, the paint-brushed devices took several minutes to dry.

2.1.5 Metal Evaporation

The final step in the the fabrication process for creating spin-coated and paint-brushed organic bulk heterojunction solar cell devices is depositing the top metal electrode. In the devices fabricated for this academic study, aluminum is used as the top metal electrode. Aluminum

behaves as the cathode in the organic bulk heterojunction solar cell devices fabricated in this study. In the devices fabricated for this study, aluminum extracts electrons conducted by the PCBM molecules out of the devices during the photovoltaic operation of the solar cells. Under forward bias in dark conditions, the aluminum electrode would inject electrons into the active layer of the solar cell devices.

In order to deposit the top metal electrode of the organic solar cell devices, the partially completed organic solar cell devices had to be removed from the glove box environment and taken to an external thermal metal evaporator evaporator. Normally, organic solar cell devices would have their top metal electrode layers deposited by a thermal evaporator installed in a glove box environment to avoid oxygen, moisture, and dirt exposure to the bare organic active layers of the organic solar cell devices. However, equipment availability and training dictated that an external thermal metal evaporator needed to be used for depositing the top metal electrode layer. A typical thermal evaporator works by utilizing a high level vacuum environment along with melting a desirable metal by heat induced by a large electric current to deposit metal layers upon a substrate. A thermal metal evaporator requires a chamber to hold a vacuum, a set of vacuums pumps to create and maintain a vacuum, gauges to measure a vacuum level, a stage for holding the substrate, a shutter for controlling when metal deposition occurs upon the substrate, masks for determining the evaporated layer's pattern, a power source for providing the electric current for melting and evaporating metal, a conductive boat for holding and heating the metal to be melted and evaporated, and electronics for measuring how much metal has been deposited upon the substrate. The thickness of the resulting thermally evaporated metal layer is measured and monitored using a quartz crystal microbalance thickness monitor. Quartz is a piezoelectric material that oscillates with an applied varying electric field. As metal is deposited upon the substrates, metal is also deposited upon the quartz crystal microbalance, dampening the resonate oscillating frequency of the quartz crystal. The changes in the resonate oscillating frequency of the quartz crystal microbalance correspond to changes of film thickness upon the quartz crystal, allowing metal thicknesses to be measured and reported throughout the metal evaporation process.

The thermal evaporator system used for depositing the top metal electrode of the organic

bulk heterjunction solar cells in this study is comprised of vacuum equipment and electrical equipment described, in general, in the above paragraph. The main structure of the thermal metal evaporator is comprised of a large metal chassis, which serves to support and connect a large turbo-molecular pump and a large glass chamber for holding the high level vacuum during the metal evaporation. The chassis also incorporates a stage for holding the substrate to be evaporated, a pattern mask, and the thickness monitor. A shutter is also attached to the chassis of the thermal evaporator system The vacuum system of the thermal evaporator includes a Welch Duo-Seal Model 1397 mechanical pump, a Leybold-Heraeus Trivac Model D30A mechanical pump, and a large Leybold-Heraeus turbo-molecular pump. The Welch Duo-Seal mechanical pump is used for establishing a low enough vacuum to engage the large turbo-molecular pump. The large Leybold-Heraeus turbo-molecular pump is used to provide and maintain the high level vacuum required for metal deposition. The Leybold-Heraeus Trivac mechanical pump is utilized as a backing pump for the large Leybold-Heraeus turbo-molecular pump, providing the exhaust for the vacuum system. A MKS Type 290 Ion Gauge Controller is used to report readings of the vacuum level of the metal deposition chamber from a hot filament ionization gauge connected to the deposition chamber. The vacuum chamber also contains the electrical connections for connecting a tungsten boat that holds the aluminum metal wire to be melted for the evaporation. The electronics on the outside of the vacuum chamber for the metal evaporator include: an MKS Type 290 Ion Gauge Controller, a Maxtek Model TM-200R Thickness Monitor, a Leybold-Heraeus Turbotronik NT 1500 turbo pump controller, and a PowerStat Type 136 Variable Autotransformer. The transformer used in the metal evaporator setup described is a step-down transformer used to boost the current flowing though the tungsten boat for heating purposes.

The procedures for evaporating aluminum films onto the paint-brushed and spin-coated devices in this study include, cleaning the evaporation chamber, loading the necessary material into the evaporation chamber, establishing a vacuum in the evaporation chamber, and evaporating the metal in a controlled fashion to yield highly conductive metal films. First, the evaporation chamber is cleaned using isopropanol. Next, the pattern mask, solar cell devices, and tungsten boat with the aluminum wire source material are installed. The next step in the

metal evaporation process is to establish vacuum within the evaporation chamber. Typically, purging and evacuating the chamber is utilized to quickly establish a high level vacuum. Initially, three nitrogen purges are performed on the evaporation chamber using only the roughing mechanical pump. After the initial roughing purges, the evaporation chamber undergoes seven to ten nitrogen purges involving the turbomolecular pump. After the nitrogen purges, the evaporation chamber is evacuated by the turbomolecular pump for approximately an hour. Once a suitable vacuum is achieved within the evaporation chamber, the aluminum metal wire is melted by using current from the step-down transformer. As the melted aluminum is heated, it evaporates up towards the solar cell device, forming a top metal electrode. The pressures utilized during the metal evaporation process are typically on the order of $2X10^{-6}$ Torr. Evaporation rates are usually kept around 20Å/s to avoid aluminum oxide barriers in the metal films being deposited on the solar cell devices in this study. The aluminum metal film thickness for the devices in this study is 200nm. Figure 2.1 shows an illustration of a cross section of the layer architecture used for the organic solar cell devices in this study. Figure 2.2 shows a photograph of a spin-coated device fabricated for this study. Figure 2.3 shows a photograph of a paint-brushed device fabricated for this study. As can be seen in Figure 2.2 and Figure 2.3, the paint-brushed device shows excessive PCBM agglomeration within the active layer film of the device.

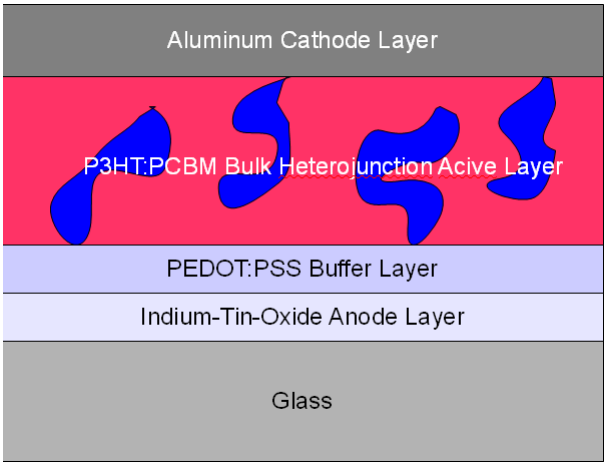

Figure 2.1 An Illustration of the Completed Organic Bulk Heterojunction Architecture

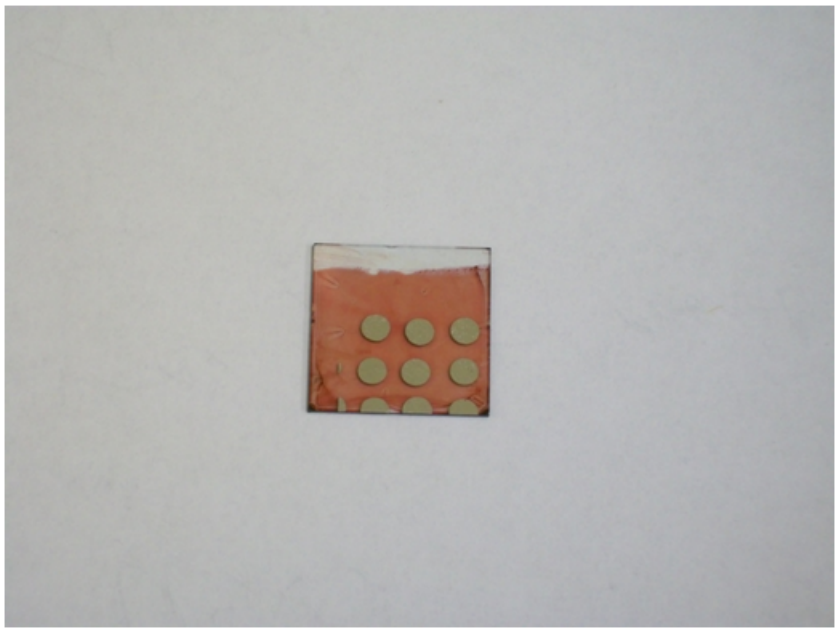

Figure 2.2 A Photograph of a Fabricated Spin-Coated Organic Bulk Heterojunction Solar Cell

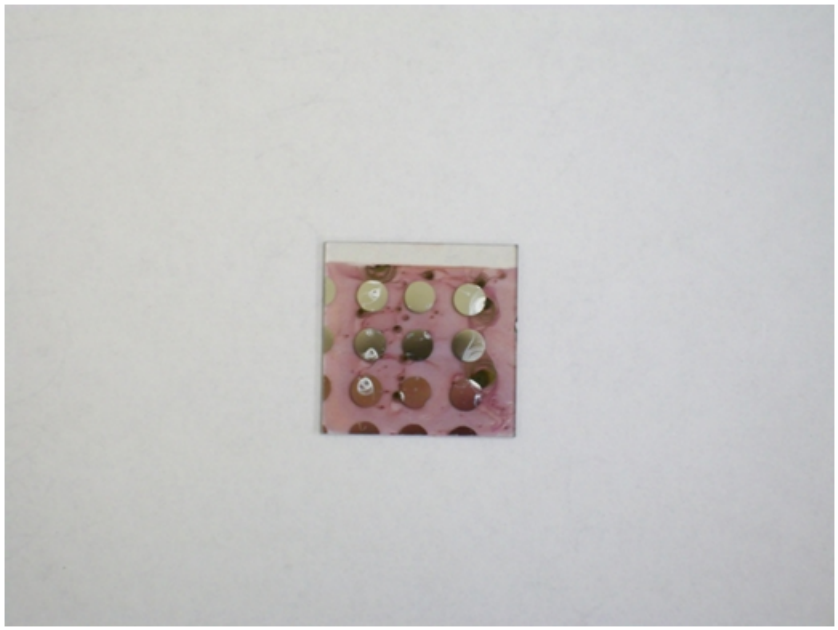

Figure 2.3 A Photograph of a Fabricated Paint-Brushed Organic Bulk Heterojunction Solar Cell

2.2 Device Characterization

This section of Chapter 2 details the methods for experimentally characterizing the spin-coated and paint-brushed organic solar cell devices fabricated for this academic study. The theory and reasoning behind each of the characterization methods will be presented. The experimental device characterization apparatuses will be fully detailed, including descriptions of equipment used within the apparatuses. The data obtained from the experimental device characterization will be analyzed in a later chapter.

2.2.1 Light Current-Voltage

The most important set of data for all fields of photovoltaics is the measured current for applied voltage under illumination of light for solar cell devices, henceforth to be referred to as "light current-voltage" measurements. Light current-voltage measurements are important because they convey a lot of information about the operation of the solar cell. Many parameters of a solar cell device can be extracted from light current-voltage measurements, such as power conversion efficiency, fill factor, short circuit current, and open circuit voltage. The equation of a solar cell's fill factor can be seen in Equation (2.1), where V_m, I_m, V_{oc}, and I_{sc} are, respectively, the voltage at the maximum output power point, the current at the maximum output power point, the open circuit voltage, and the short circuit current obtained from a solar cell's light current-voltage measurements [1]. The equation for the power conversion efficiency in a solar cell device can be seen in Equation (2.2), where P_{in} is the input power from the solar cell's illumination source [1]. In a laboratory setting, usually a light source of 100mW/cm^2, or one "Sun's", worth of light power flux with an Air Mass 1.5 Global (AM 1.5G) light spectrum is utilized for conducting light current-voltage measurements.

$$FF = \frac{V_m I_m}{V_{oc} I_{sc}} \tag{2.1}$$

$$\eta_e = \frac{V_{oc} I_{sc} FF}{P_{in}} \tag{2.2}$$

The series resistance and shunt resistance can also be qualitatively analyzed by viewing the plot of light current voltage measurements. The series and shunt resistances in solar cell devices

are qualitatively analyzed from light current-voltage measurements by evaluating the slopes of the plot of the light current-voltage measurements at the x-axis(voltage axis) intercept and y-axis(current axis) intercept, respectively. A high slope at the y-axis(current-axis) intercept, when evaluated from the y-axis, corresponds to a large shunt resistance, which is desirable in solar cells. Conversely, a high slope at the x-axis(voltage-axis) intercept, when evaluated from the x-axis, corresponds to a low series resistance, which is desirable in solar cells. To quantitatively estimate the series and shunt resistance of a solar cell, the slopes of the plot of light current-voltage measurements can be calculated at the x-axis(voltage-axis) intercept and at the y-axis(current axis) intercept to quantitatively estimate, respectively, the series resistance and shunt resistance of the solar cell, if carrier collection is not dependent on an applied bias. However dark current voltage measurements are more commonly used to extract the series resistance and shunt resistance of a solar cell.

The equipment utilized for the taking the light-current voltage measurements in this study includes: a computer, a source-measure unit, an ELH bulb illumination source, a power supply, a reference solar cell, and measurement probes. The solar cell architecture utilized for the organic solar cell devices in this study is referred to as a superstrate architecture, an architecture requiring illumination to be incident upon the bottom of the solar cell structure. The light current-voltage measurement setup includes a stage with a hole in it to allow the light source to illuminate the organic solar cell devices in this study from the bottom. An ELH bulb was used to provide the illumination source approximating one Sun's worth of solar flux. A pair of Wentworth Labs PRO191 measurement probes were used to measure the electrical current outputted from the solar cell devices under illumination. A Keithley 236 Source-Measure Unit is utilized to source voltages to the solar cells under illumination while at the same time measuring the currents produced by the solar cell devices. A computer connected to the Keithly 236 has a Keithly program installed that automates the taking of light current-voltage measurements. A Hewlett Packard 6443B DC Power Supply provided power to the ELH bulb illumination source. A reference solar cell with a known short-circuit current at one Sun's illumination was used to calibrate the illumination output from the ELH bulb.

2.2.2 Dark Current-Voltage

A very important measurement for analyzing solar cell devices is the measurement of current for applied voltage under dark conditions, henceforth to be referred to as "dark current-voltage" measurements. Dark current-voltage measurements can provide a lot of information without the need for an expensive solar simulator setup. A few solar cell parameters that dark current-voltage measurements can be used to help estimate are shunt resistance, series resistance, diode ideality factor, and reverse saturation current. Usually, an equivalent circuit model us utilized to evaluate extract the previously mentioned device parameters. Figure 2.4 shows an equivalent circuit model for evaluating dark current-voltage measurements. As can be seen in Figure 2.4, the equivalent circuit for evaluating dark current-voltage measurements takes into account series resistance, shunt resistance, and space charge limited current effects. The equivalent circuit for evaluating dark current-voltage measurements also takes into account recombination/generation current effects by including a second diode. Some solar cells can be modeled with just using one diode; others require the second diode to model the recombination/generation current effects. If the dark current-voltage plot shows an "s-shape" curve, then the two diode model is required to accurately model the solar cell device. For the purposes of this study, dark current-voltage measurements were only made to analyze electron injection at the aluminum contacts for both spin-coated and paint-brushed devices.

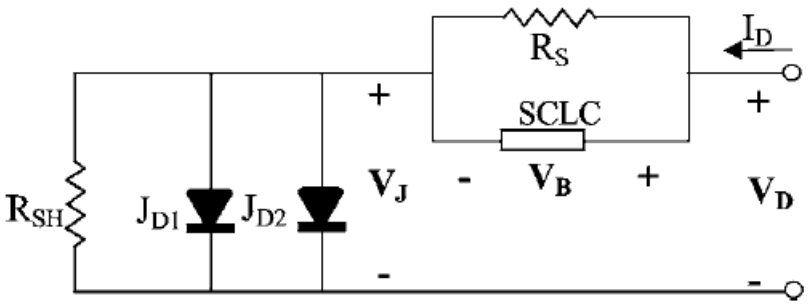

Figure 2.4 Equivalent Circuit for Dark Current-Voltage Measurements [47]

The equipment utilized in the dark current-voltage measurement setup includes: a programmable voltage source, an electrometer, a set of measurement probes, a dark box, and a

computer. The dark current-voltage setup includes a darkbox for storing the sample during the dark current-voltage measurements. A set of Wentworth Labs PRO191 measurement probes are set up within the darkbox to measure current from the solar cell devices for dark current-voltage measurements. A Keithly 230 Programmable Voltage Source is utilized to source voltage to the solar cell devices during dark current-voltage measurements. A Keithly 617 Programmable Electrometer is utilized to measure the very low currents produced from the solar cells during dark current-voltage measurements. A computer with a custom-built software program automates the measurement process for dark current-voltage measurements.

2.2.3 Quantum Efficiency

Quantum efficiency measurements are important measurements for classifying the photonic spectral performance of solar cell devices. The quantum efficiency for solar cell devices is defined as the ratio of the number of charged carriers extracted, or collected, from the solar cell to the number of photons of a given wavelength shining on the solar cell. The quantum efficiency of solar cell devices is also referred to as **I**ncident-**P**hoton-to-Electron-**C**onversion-**E**fficiecny (IPCE). Quantum efficiency measurements can be classified as either **E**xternal **Q**uantum **E**fficiency (EQE) measurements or **I**nternal **Q**uantum **E**fficiecny (IQE) measurements. The external quantum efficiency of a solar cell device is defined as ratio of charged carriers collected to the number of incident photons of a given wavelength shining on the solar cell, basically the same definition as for quantum efficiency. The internal quantum efficiency of a solar cell device is defined as the ratio of the number of charged carriers collected to the number of incident *absorbed* photons of a given wavelength. The reflectance and transmission of incident photons shining on the solar cell device must be measured in order to calculate internal quantum efficiency measurements from measured external quantum efficiency measurements.

Quantum efficiency measurements provide data that show the photonic spectral sensitivity of a solar cell device. External quantum efficiency measurements provide information on generated charged carrier collection with respect to all photons incident upon the solar cell device. Internal quantum efficiency measurements provide information on generated charged carrier collection with respect to only absorbed photons incident upon the solar cell device. By

definition, internal quantum efficiency is always larger than external quantum efficiency due to the fact that external quantum efficiency measurements take into account all incident photons while internal quantum efficiency measurements only take into account absorbed photons. Low internal quantum efficiency measurements indicate generated charged carrier collection issues. Low external quantum efficiency measurements can be indicative of high incident photon reflection, poor generated charged carrier collection, or high incident photon reflection coupled with poor generated charge collection.

Quantum efficiency measurements are made by measuring the short circuit current of a solar cell device while shining monochromatic light upon the solar cell being measured. The monochromatic light used for measuring the quantum efficiency of a solar cell device is usually produced from light selected by a monochromator from a halogen bulb light source. Quantum efficiency measurements are often measured in normal lighting conditions, which add a considerable amount of noise to the resulting measurements. To eliminate the effect of ambient lighting on the quantum efficiency measurements of a solar cell, a lock-in amplification technique is employed. The lock-in amplification technique for measuring the quantum efficiency of a solar cell device involves using a pre-amplifier, a lock-in amplifier, and an optical chopper for chopping the light outputted from the monochromator. Lock-in amplifiers are usually used to extract signals from measurements with low signal-to-noise ratios. A lock-in amplifier works by integrating the product of a reference signal and a measured input signal and outputting the resulting value. The resulting output of a lock-in amplifier is a DC voltage when the reference signal and input measurement signal are in phase and of the same frequency. Due to the orthogonality of sinusoidal signals, all of the measurements with frequencies not equal to the reference signal, in other words the noise, will be severely attenuated, leaving the DC voltage output mostly representative of the desired measurement. To produce a time-varying short circuit current signal from a solar cell device for quantum efficiency measurements, an optical chopper is used to the chop the light outputted from the monochromator. The light outputted from the monochromator is operated at a specific frequency that matches the reference frequency inputted to the lock-in amplifier, a requirement for the lock-in amplification technique. The resulting time-varying short circuit current from the solar cell due to the illumination of the

chopped monochromatic light is inputted into a transimpedance pre-amplifier and converted into a voltage that can be processed by the lock-in amplifier. The resulting output of the lock-in amplifier from the signal inputted from the transimpedance pre-amplifier, which, in turn, was provided a signal from the solar cell device under investigation, provides the necessary data for quantum efficiency measurements.

The quantum efficiency measurements measured for the solar cell devices in this study are considered "relative" external quantum efficiency measurements. The quantum efficiency measurements are considered relative quantum efficiency measurements because the measurements are compared to the measurements of a reference solar cell with a known measured quantum efficiency. Using the lock-in amplifier technique described in the above paragraph, the short-circuit currents are measured for a reference solar cell with a known quantum efficiency initially. Once measurements have been made for the reference solar cell, short-circuit current measurements are made for the solar cell being investigated. As described in the above paragraph, the short-circuit current measurements for both the reference solar cell and the solar cells under investigation are converted into voltages by a transimpedance pre-amplifier and inputted into the lock-in amplifier. The output of the lock-in amplifier provides voltage data for each photonic wavelength utilized for the quantum efficiency measurements. To determine the relative external quantum efficiency of the solar cell device being investigated, the ratio of the measured voltages corresponding to each photonic wavelength measured for quantum efficiency for both the reference solar cell and the solar cell under investigation are taken and multiplied by the known quantum efficiency of the reference solar for each photonic wavelength applicable. Unfortunately, the area of illumination by the monochromatic light is unknown for both the reference solar cell and the solar cell being investigated. To take into account the unknown areas of illumination for the solar cells involved in quantum efficiency measurements, the quantum efficiency measurements for the solar cell under investigation are normalized to 90%. Equation (2.3) shows the equation used for the calculation of the realtive external quantum efficiency of a solar cell device. The normalization process involved for the quantum efficiency measurements is conducted by a computer program that sets the peak quantum efficiency meaurement to 90% and normalizes all other quantum efficiency measurements with respect to

that peak quantum efficiency measurement.

$$E.Q.E._{relative} = E.Q.E._{ref} \left(\frac{V_{sample}}{V_{ref}} \right) \tag{2.3}$$

The quantum efficiency measurement system used for measuring the solar cells in this study is nearly fully automated by a computer program developed by graduate students at the Microelectronics Research Center at Iowa State University. The computer program controls the monochromator, lock-in amplifier, and a voltage source for applying a bias to the solar cell under investigation. The monochromator used in this system is a ISA Jobin Yvon H20 single-grating monochromator. The lock-in amplifier used in the quantum efficiency measurement system is a Stanford Applied Research Systems Model SR830 DSP Lock-In Amplifier. An Ithaco Model 1211 Current Pre-amplifier is used for converting the short-circuit current measurements for each wavelength of light tested from the solar cell device being investigated into a voltage for input into the lock-in amplifier. The optical chopper used in the quantum efficiency measurement system is a Thor Labs MC1000A optical chopper, which comes with a controller as well. The optical chopper is operated at a frequency of 13Hz, as this frequency is not a known harmonic of any other signal produced in the lab. A set of two optical filters is used for the quantum efficiency measurements for specific measurement ranges of photonic wavelengths in order to eliminate second order diffraction effects. For high photon wavelength measurements, a 700nm long-pass optical filter is used to filter photons of lower wavelengths that may be passed by the monochromator due to second order diffraction effects. For low photon wavelengths, a 580nm short-pass filter is used to filter photons of higher wavelengths that may be passed by the monochromator due to second order diffraction effects. The solar cell devices in this study had their relative external quantum efficiencies measured for light wavelengths of 400nm-800nm.

2.2.4 Absorbance

Absorption is an important measurement for solar cell devices. Absorption is defined as the percentage of incident photons absorbed by a material. Unfortunately, absorption cannot be directly measured by any type of measurement equipment. Instead, absorption must be inferred

from measurements of photon reflection and photon transmission for materials. Reflection is defined as the percentage of incident photons upon a material that are reflected from the material. Likewise, transmission is defined as the number of incident photons upon a material that are transmitted through the material. Absorption, reflection, and transmission usually have different values for different photon wavelengths for a specific material. For instance, the energy band gap of a material heavily defines which photons may be absorbed by that material. Most photo-spectrometers actually measure transmission only. Transmission measurements can be transformed into absorbance values by using Equation (2.4). Absorbance is also known as optical density, a term used for optical filters. Absorbance measurements have been used to provide evidence of polymer crystallinity and enhanced polymer conjugation lengths in organic photovoltaic films [27].

$$Absorbance = \log\left(\frac{1}{T}\right) \tag{2.4}$$

For the purposes of this study, absorbance measurements were conducted on organic photovoltaic films fabricated by spin-coating and brush-painting. A Varian Cary 5000 Spectrophotometer that is capable of providing absorbance measurements for ultraviolet, visible, and near infrared photons was used to conduct the absorbance measurements on the organic solar cell devices investigated in this study. The Varian Cary 5000 spectrophotometer utilizes two diffraction gratings along with a halogen bulb to realize photon wavelengths from 175nm to 3300nm, covering the ultraviolet, visible, and near infrared photonic spectrums. A single photodiode is utilized by the Varian Cary 5000 photospectrometer for measuring the absorbance of a material. A complicated network of mirrors within the Varian Cary 5000 directs a light beam of a certain photon wavelength through a sample under investigation to a photodiode to measure the transmission through the sample under investigation. To fully measure the photonic transmission of a sample under investigation, an unimpeded beam of light of the same wavelength must also be measured by the photodiode to provide a reference for the measurement taken with the sample impeding the beam of light. In order to provide photodiode measurements for both impeded and unimpeded beams of light, the Varian Cary 5000 is setup with an optical chopper that chops the light at a certain frequency. The chopper is a mirror that directs the source beam of light towards a network of mirrors that further directs the beam of light towards

and through a sample under investigation. When the chopper allows the source beam of light through, the beam of light is directed to another network of mirrors that directs the beam of light to the photodiode, unimpeded by the sample under investigation. Because only one photodiode is utilized for measuring the sample-impeded and unimpeded photoresponses, the two beam signals must be separated in phase to avoid interference. The chopper also serves to provide the time varying input signal for a lock-in amplification technique for measuring the photoresponses of the photodiode in the Varian Cary 5000, similar to the lock-in amplification technique previously explained for measuring the quantum efficiency of solar cell devices.

2.2.5 Atomic Force Microscopy

Atomic Force Microscopy is an important surface profiling technique for researchers in the organic photovoltaics research field. Atomic force microscopy allows for nanometer level resolution measurements of surface roughness, phase imaging, and thickness. Atomic force microscopy utilizes the reflection and detection of light in order to determine surface roughness, phase grain size, and film thickness from thin films. An atomic force microscope is comprised of a piezoelectric stage, an incredibly small profiling tip, a red laser, a set of photodetectors, and a computer system. An atomic force microscope operates by rastering a thin film sample under a profiling tip by applying voltages to the piezoelectric stage. During the rastering process, a red laser is shined on the profiling tip. A set of photo detectors detect the reflected laser light from the profiling tip during the rastering process, providing a set of information used in surface profile imaging and phase imaging. A Veeco MultiMode atomic force microscope was used in this study to produce micrographs of surface roughness, phase, and film thickness for both spin-coated and paint-brushed devices. The tapping mode atomic force microscope scanning technique was used for producing the AFM micrographs in this study. The tapping mode technique involves having the profiling tip tap along the surface of the films, instead of being dragged along the films. The tapping mode technique helps prevent damage to the organic films being studied. To determine the thicknesses of the paint-brushed and spin-coated films in this study, a syringe needle was used to create a trench for profiling.

CHAPTER 3. DATA ANALYSIS

3.1 Light Current-Voltage

Light current-voltage measurements were measured using the equipment and techniques presented in Section 2.2.1. For this academic work, four sets of organic bulk heterojunction solar cell devices were fabricated, with each set comprising devices on an indium tin oxide coated glass slide. Two sets of organic bulk heterojunction solar cell devices were fabricated by paint brushing the active layer, as described in Section 2.1.4. The other two sets of organic bulk heterojunction solar cell devices were fabricated by spin coating the active layer, also as described in Section 2.1.4. Tables 3.1, 3.2, 3.3, 3.4 show a data summary for the parameters: Voc, Jsc, fill factor, and power conversion efficiency, respectively, extracted from analyzing light current-voltage measurements performed on the devices. As can be seen in the data summary tables, the paint-brushed devices are nearly twice as power efficient as the spin-coated devices. However, the power efficiencies from all of the sets of devices are extremely poor, at nearly an order of magnitude lower than reported power conversion values found in literature [26]. The fill factors for the paint-brushed devices and spin-coated devices were found to be around 50 and 30, respectively. The open-circuit voltages for the paint-brushed devices were consistently around 0.38V. The spin-coated devices exhibited more variation in open circuit voltage, with voltages ranging from 0.48V to 0.62V. The open circuit voltages for the paint-brushed devices are uncommonly low compared to reported values found in literature [26]. The low open circuit voltages of the paint-brushed devices may be due to unknown effects of exposing bare organic films to the ambient atmosphere before depositing the top metal electrode. The relatively high open circuit voltages of the spin-coated devices are most likely due to low dark currents and correspondingly low reverse saturation currents due to high series resistance and poor device

fill factors. The short circuit current in the paint-brushed devices was found to be larger than the the short circuit currents in the spin-coated devices by 1mA/cm^2 on average. The short circuit currents for both devices are also considered low compared to reported values found in the literature [26].

Table 3.1 Voc Data Summary For Paint-Brush and Spin-Coated Organic Solar Cells

Device Set	**Min. Voc (V)**	**Max. Voc (V)**	**Avg. Voc (V)**
Spin-coated 1	0.4775	0.6192	0.5696
Spin-coated 2	0.4381	0.4666	0.4523
Paint-brushed 1	0.3611	0.3878	0.3763
Paint-brushed 2	0.3764	0.3878	0.3809

Table 3.2 Jsc Data Summary For Paint-Brush and Spin-Coated Organic Solar Cells

Device Set	**Min. Jsc(mA/cm^2)**	**Max. Jsc(mA/cm^2)**	**Avg. Jsc(mA/cm^2)**
Spin-coated 1	1.417	2.014	1.773
Spin-coated 2	1.871	2.436	2.132
Paint-brushed 1	2.755	3.479	3.185
Paint-brushed 2	2.715	3.089	2.874

Table 3.3 Fill Factor Data Summary For Paint-Brush and Spin-Coated Organic Solar Cells

Device Set	**Min. FF. (%)**	**Max. FF. (%)**	**Average FF. (%)**
Spin-coated 1	32.27	44.12	35.09
Spin-coated 2	27.05	31.07	28.44
Paint-brushed 1	49.07	52.52	50.72
Paint-brushed 2	50.56	52.12	51.19

The difference in device performance between spin-coated and paint-brushed solar cell devices is clearly evident from the plotted curves in Figure 3.1. Figure 3.1, shows a sample of two light current-voltage curves, one each from a paint-brushed device and a spin-coated device. Due to the fact that the spin-coated and paint-brushed devices showed self-consistency throughout device sets, only a small sampling is necessary to illustrate the difference between the two types of devices. As can be seen in Figure 3.1, the paint-brush device exhibits a more ideal solar cell light current-voltage characteristic. On the other hand, the spin-coated solar cell device exhibits very poor performance, showing a "S-shaped" light current-voltage characteris-

Table 3.4 Efficiency Data Summary For Paint-Brush and Spin-Coated Organic Solar Cells

Device Set	**Min. Eff. (%)**	**Max. Eff. (%)**	**Average Eff. (%)**
Spin-coated 1	0.274	0.401	0.352
Spin-coated 2	0.255	0.303	0.273
Paint-brushed 1	0.524	0.686	0.609
Paint-brushed 2	0.517	0.624	0.561

tic. Typically, "S-shaped" curves for solar cell light current-voltage measurements correspond to internal device potential barriers preventing charged carriers from being extracted at the electrodes.

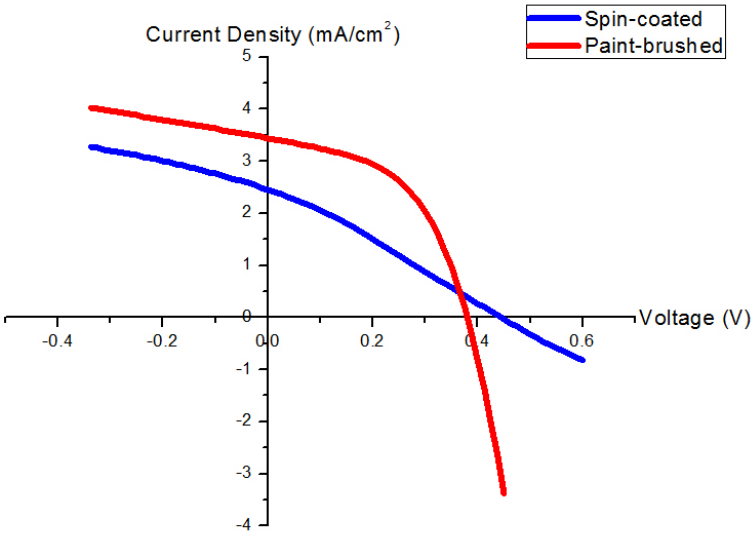

Figure 3.1 Light Current-Voltage Comparison of Paint-Brushed and Spin-Coated Devices

In 2009, Villers et al. found that small changes in solvent evaporation kinetics can lead to devices that exhibit "S-shaped" light current-voltage characteristics during an investigation of reproducibility of organic solar cell device performance [48]. In their study, Villers et al. determined that unwanted vertical phase separation of PCBM molecules towards the anode electrode, which is usually indium tin oxide for most organic solar cell applications, created a barrier to electron extraction at the cathode, which is usually the top metal electrode. Figure 3.2 shows a diagram illustrating unwanted vertical phase separation of PCBM in organic bulk

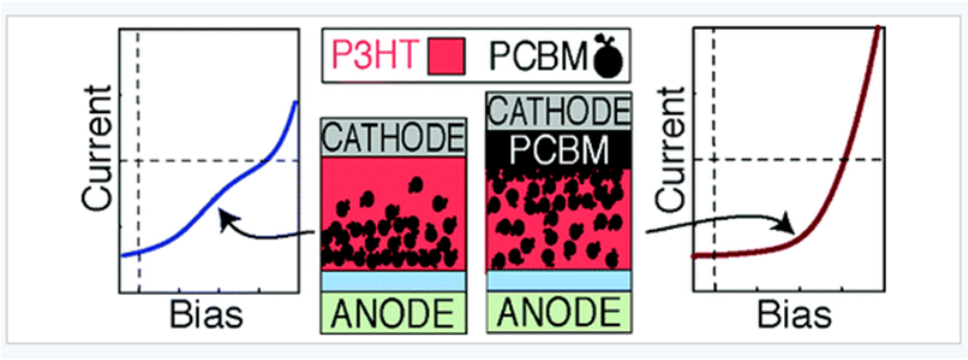

Figure 3.2 Illustration of Unwanted PCBM Vertical Phase Separation in Organic Solar Cells [48]

heterojunction devices. During the fabrication of the organic solar cell devices, a slower drying time was noticed with paint-brushed samples when compared to the drying times of spin-coated samples. Based on the study done by Villers et al., the most likely cause of the "S-shaped" curve of spin-coated solar cell devices in this study is unwanted vertical phase separation of PCBM molecules in the organic solar cell films towards the anode due to the faster drying time for spin-coated devices. Li et al. found that slower film drying times and, correspondingly, slower solvent annealing for organic bulk heterojunction films lead to better, more crystalline devices [27]. In this study, the slower drying, slower solvent annealing, paint-brushed devices must exhibit better crystallinity and better self-assembled nano-morphology, with less unwanted vertical phase separation of PCBM molecules in the active layer films when compared to the spin-coated devices. Although the light current-voltage data strongly suggests unwanted vertical phase separation of PCBM molecules in spin-coated, more experimental data needs to be shown to prove the hypothesis.

3.2 Dark Current-Voltage

Dark current-voltage measurements were measured using the equipment and techniques presented in Section 2.2.2. Figure 3.3, shows dark current-voltage measurements for a paint-brushed organic solar cell device and a spin-coated organic solar cell device. Device sets from both paint-brushed and spin-coated devices showed self consistent behavior. Therefore, only

results from one device from both paint-brushed and spin-coated device sets are necessary to make a comparison. Fully evaluating and extracting the parameters of a solar cell device requires an involved mathematical process, usually requiring a mathematical software package. Fortunately, for the purposes of this study, a full analysis of the solar cell devices is not required. From the light current-voltage analysis, it was clearly evident that the spin-coated devices suffered from a large series resistance, most likely due to unwanted vertical phase separation of PCBM molecules in the device's active layer. Dark current-voltage measurements can qualitatively provide information on charge injection and about the difference in reverse saturation current between the two types of devices. As can be see in Figure 3.3, the dark current for the paint-brushed organic solar cell devices is nearly two magnitudes greater than the dark current for the spin-coated device. This observation shows that the spin-coated device has an issue with injecting charges under forward bias. Most likely, electron injection from the top metal cathode electrode is inhibited by a potential barrier due to the overabundance of polymer molecules near the top metal cathode electrode. This overabundance of the electron donor polymer molecules must be a result of unwanted vertical phase separation of the electron acceptor PCBM molecules.

$$J_D = J_0 \left(\exp \frac{qV}{nkT} - 1 \right) \tag{3.1}$$

$$V_{oc} = \frac{kT}{q} \ln \left(\frac{J_{sc}}{J_0} + 1 \right) \tag{3.2}$$

The low dark current of the spin-coated devices explains the relatively high open circuit voltages of the spin-coated devices. Equation 3.2 shows the equation for the open circuit voltage of a solar cell [49]. As can be seen from Equation 3.2, open circuit voltage is dependent upon the reverse saturation current of a solar cell. Equation 3.1, shows the famous Shockley diode equation [49]. The Shockley diode equation shows that dark current will be dependent upon the magnitude of the reverse saturation current, J_0. The spin-coated solar cell devices show a low reverse saturation current due to their overall low dark current. Correspondingly, the spin-coated devices exhibit a larger open circuit voltage than the paint-brushed devices, which exhibit higher dark currents and higher reverse saturation currents.

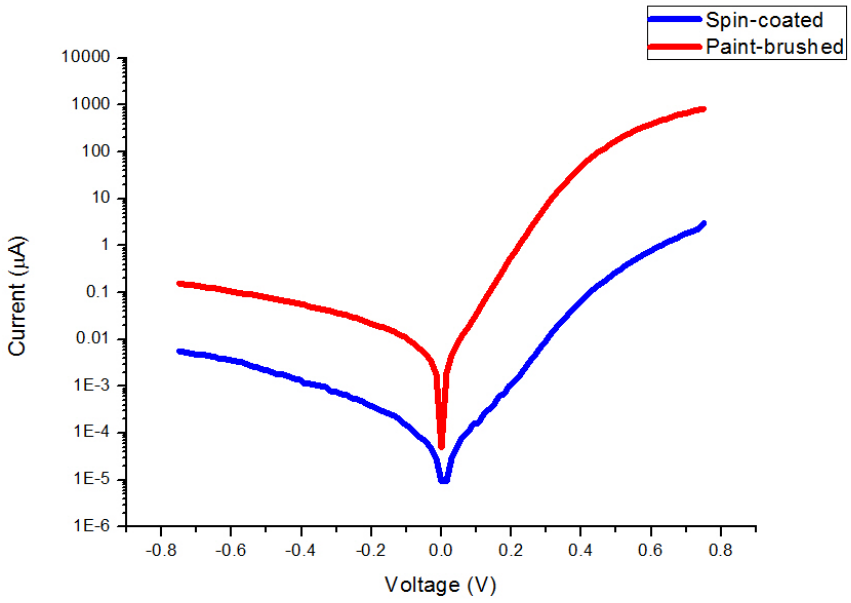

Figure 3.3 Dark Current-Voltage Comparison of Paint-Brushed and Spin-Coated Devices

3.3 Absorbance

Absorption is an important property of active layer films in solar cell devices. Absorption provides an indication of how much light is absorbed in the active layer films of solar cell devices for each photon energy within the solar light spectrum. Typically, high absorption is desirable for harvesting solar light energy, up to a point. However, photons with energies greater than the energy band gap of the materials comprising the active layers of solar cell devices convert most of their energy to heat by interacting with the material lattice within the active layer and creating of phonons in the process, which increases the series resistance of solar cell devices. Unfortunately, absorption is not directly measurable, and, instead, it must be inferred from transmission and reflectance measurements. Absorbance, which is actually a measurement of transmission, is frequently reported as an approximation for light absorption within active layers of organic solar cells in organic photovoltaic literature. The absorbance measurements reported in this study were measured using the equipment and techniques described in Section 2.2.4.

Figure 3.4 shows the measured absorbance characteristics for organic bulk heterojunction active layers fabricated by spin coating and brush painting. Device sets from both paint-

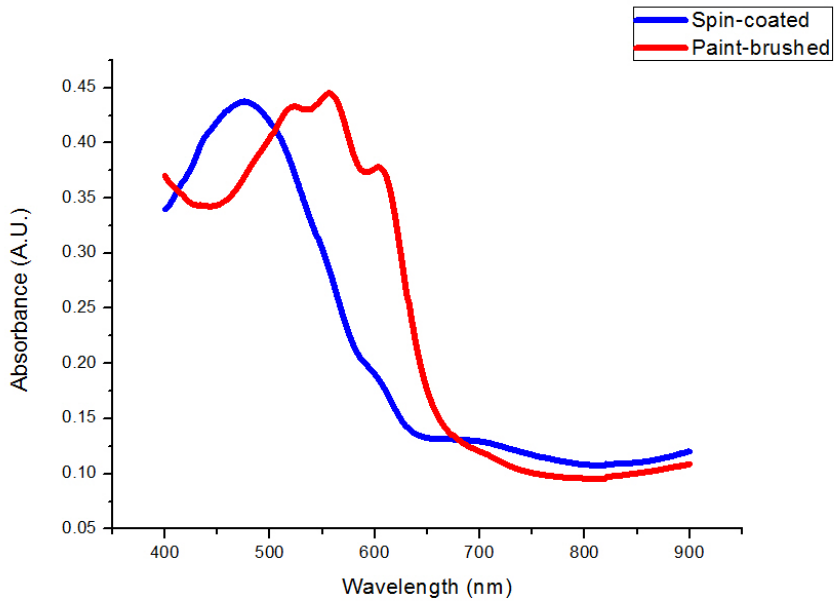

Figure 3.4 Absorbance Comparison of Paint-Brushed and Spin-Coated Devices

brushed and spin-coated devices showed self consistent behavior with regards to absorbance measurements, so only a small sample is required to illustrate the differences in absorbance between organic solar cell devices fabricated by paint brushing and spin coating. As can be seen in Figure 3.4, the paint-brushed organic solar cell device exhibits a significant red-shift in absorbance with respect to the absrobance of the spin-coated organic solar cell device. Also, as can be seen in Figure 3.4, the paint-brushed organic solar cell device has a measured absorbance characteristic showing three pronounced vibronic absorbance shoulders, whereas the spin-coated device does not exhibit these absorbance shoulders as much. Red light absorption is desired in solar cell devices for harvesting more photonic power from the solar light spectrum. Also, certain applications, such as photoluminescence-based oxygen sensing, require photodetectors with decent red light absorption, making the paint-brushed organic solar cell devices in this study highly desirable if they are able to collect the photo-induced charges from red photons.

Li et al. conducted a study on solvent annealing spin-casted organic bulk heterojunction solar cell devices in 2009 [27]. Li et al. found that solvent annealing slowed down the organic bulk heterojunction active layer film drying times, resulting in better solar cell device performance

with better red light absorption. The better red light absorption, along with the well defined three vibronic absorption shoulders, was attributed by Li et al. to be due to the higher polymer conjugation within the solvent annealed organic bulk heterojunction solar cells as a result of the slower drying times. The slower drying times of the solvent annealed organic bulk heterojunction solar cells reported on by Li et al. allowed for an efficient nano-scale morphology featuring a more crystalline polymer phase incorporating enhanced polymer conjugation. The solvent annealing study reported on Li et al. parallels the research presented in this study. The active layers of the paint-brushed organic solar cells in this study dried much slower than the active layers of the spin-coated devices. The active layers of the spin-coated devices in this study were essentially dry coming off the wafer chuck immediately after spin coating. As was seen in the solvent annealing study that Li et al. conducted, the slower dried organic bulk heterojunction solar cells in this study, or the paint-brushed devices, exhibited more red absorbance with enhanced vibronic shoulders. The enhanced red absorbance in the paint-brushed devices in this study is most likely due to the slower active layer drying times resulting in desirable nano-scale morphologies featuring enhanced crystallinity and polymer conjugation within the polymer phases of the bulk heterojunctions.

3.4 Quantum Efficiency

The theory governing quantum efficiency measurements was described in Section 2.2.3. The equipment and measurement setup for solar cell quantum efficiency measurements were also described in Section 2.2.3. The quantum efficiency measurements made for the paint-brushed and spin-coated organic solar cell devices in this study were external quantum efficiency measurements. Furthermore, the external quantum measurements made in this study are relative external quantum efficiency measurements due to the fact that a reference solar cell with a known quantum efficiency was used for calculating the quantum efficiencies for the solar cells in this study. The quantum efficiencies measured in this study are also normalized such that the peak quantum efficiency is set at 90% with all other quantum efficiency measurements normalized to that peak quantum efficiency measurement. As described in Section 2.2.3, the normalization is carried out on the quantum efficiency measurements in order to account for

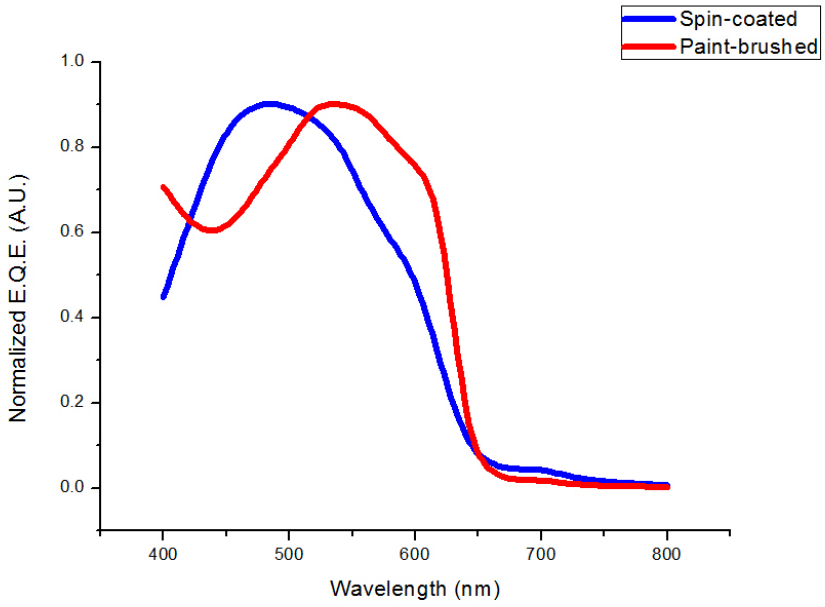

Figure 3.5 Normalized External Quantum Efficiency Comparison of Paint-Brushed and Spin–Coated Devices

the unknown area of illumination for both the reference solar cell and the solar cell under investigation.

External quantum efficiency measurements were conducted on both paint-brushed and spin-coated solar cell devices fabricated for this study. The quantum efficiency measurements for both the paint-brushed and spin-coated solar cell devices showed consistency from device to device. Due to the consistency of the quantum efficiency measurements for both paint-brushed and spin-coated solar cell devices, only a small sampling is needed to show the differences in quantum efficiency between the two types of organic solar cells. Figure 3.5 shows the normalized external quantum efficiency for both paint-brushed and spin-coated solar cell devices. As can be seen in Figure 3.5, the normalized external quantum efficiency measurements for the paint-brushed organic solar cell device show a significant red-shift in photo-generated charge collection when compared to the normalized external quantum efficiency measurements for the spin-coated organic solar cell device. The red-shift in quantum efficiency measurements for the paint-brushed devices could be simply due to more absorption from a thicker organic film. Atomic force microscopy would be needed to be implemented in order determine if the thickness

of the films for both the paint-brushed and spin-coated organic solar cell devices contribute to the red-shift in the paint-brushed devices. The external quantum efficiency measurements featured in Figure 3.5 support the absorbance measurements reported on in Section 3.3 by showing that the paint-brushed devices collect more photo-generated charges from red photons when compared to the spin-coated devices. The quantum efficiency measurements for the devices in this study also support the light and dark current-voltage measurements presented in Sections 3.1 and Section 3.2 by showing that photo-generated charges produced by red photons can be efficiently collected. Red photons, being of a lower energy, are absorbed near the metal cathode in organic bulk heterojunction solar cell devices. The quantum efficiency measurements of this study indicate that electrons from photo-generated excitons by red photons absorbed near the cathode in the paint-brushed organic solar cell devices are efficiently transferred to the metal cathode of the devices, indicating that a desirable PCBM interface exists at the metal cathode in paint-brushed devices.

3.5 Atomic Force Microscopy

Atomic Force Microscopy (AFM) is an incredibly useful and important measurement technology for researchers working in the field of organic photovoltaics. For this study, AFM micrographs of surface roughness, phase, and thickness were taken from spin-coated and paint-brushed organic bulk heterojunction solar cell active layer films. A description of the operation of the Atomic Force Microscope used for taking the AFM micrographs in this study can be found in Section 2.2.5. The AFM micrographs taken for this study showed consistency through multiple organic solar cell active layer samples. Due to the consistency found within organic solar cell active layer films from AFM micrographs, only a small sample of AFM micrographs are presented in this study to illustrate the differences between spin-coated and paint-brushed organic solar cell devices. Figure 3.6 and Figure 3.7 show AFM micrographs of surface roughness for both spin-coated and paint-brushed organic solar cell devices. As can be seen in Figure 3.6 and Figure 3.7, the surface roughness for the paint-brushed organic solar cell active layer film is much higher than the surface roughness of the spin-coated devices. The root-mean-square surface roughness for the spin-coated organic active layer film found in Figure 3.6 was found

to be 1.427nm, while the root-mean-square surface roughness of the paint-brushed active layer film found in Figure 3.7 was found to be 3.087nm. In their 2005 report, Li et al. found that slow drying, solvent annealed organic bulk heterojunction active layers had rougher surfaces than fast drying organic bulk heterojunction active layers [27]. Li et al. attributed the greater surface roughness in the slow drying organic active layers compared to the fast drying organic active layers with increased crystallinity and improved nano-scale morphology within the organic bulk heterojunction active layers of the slow drying solar cell devices. In this study, the paint-brushed organic solar cell devices had active layers that dried slower than those for the spin-coated organic solar cell devices. The most likely cause of the greater surface roughness within the paint-brushed active layers of organic solar cells is more self-organization of the polymer and fullerene bulk heterojunction blend, resulting in more crystalline polymer and fullerene phases.

Along with AFM micrographs of surface roughness, AFM phase micrographs and AFM thickness micrographs were also taken for both spin-coated and paint-brushed organic solar cell active layer films. Figure 3.8 and Figure 3.9 show AFM phase micrographs from active layer films from both a paint-brushed organic solar cell device and a spin-coated organic solar cell device. As can be seen in Figure 3.8 and Figure 3.9, the phase micrograph for the spin-coated active layer film, shows a more uniform phase distribution than the phase distribution shown in the micrograph for the paint-brushed organic active layer film. The spin-coated organic active layer film had a mean grain size of 1143.3nm^2, a grain size standard deviation of 2120.5nm^2, and a maximum grain size of 25367nm^2. The paint-brushed organic active layer had a mean grain size of 1385.9nm^2, a grain size standard deviation of 6730.1nm^2, and a maximum grain size of 109958nm^2. The phase distribution within the paint-brushed organic active layer appears to have a wider distribution of grain sizes including relatively large grains. The wider distribution of grain sizes within the paint-brushed organic active layer is most likely indicative of more crystalline fullerene phases and more crystalline polymer phases with enhanced polymer conjugation. Figure 3.10 and Figure 3.11 show AFM thickness micrographs of spin-coated and paint-brushed organic solar cell active layer films. A syringe needle was used to cut a trench in the organic solar cell active layers in order for the organic active layer thicknesses to be

determined. As can be seen in Figure 3.10 and Figure 3.11, the spin-coated organic solar cell active layer was slightly thicker than the paint-brushed organic solar cell active layer by about 50nm. This difference in thickness between the spin-coated and paint-brushed organic active layers supports that the increased red photon response in the paint-brushed solar cell devices presented in Section 3.3 and Section 3.4 is not due to thicker organic active layer films.

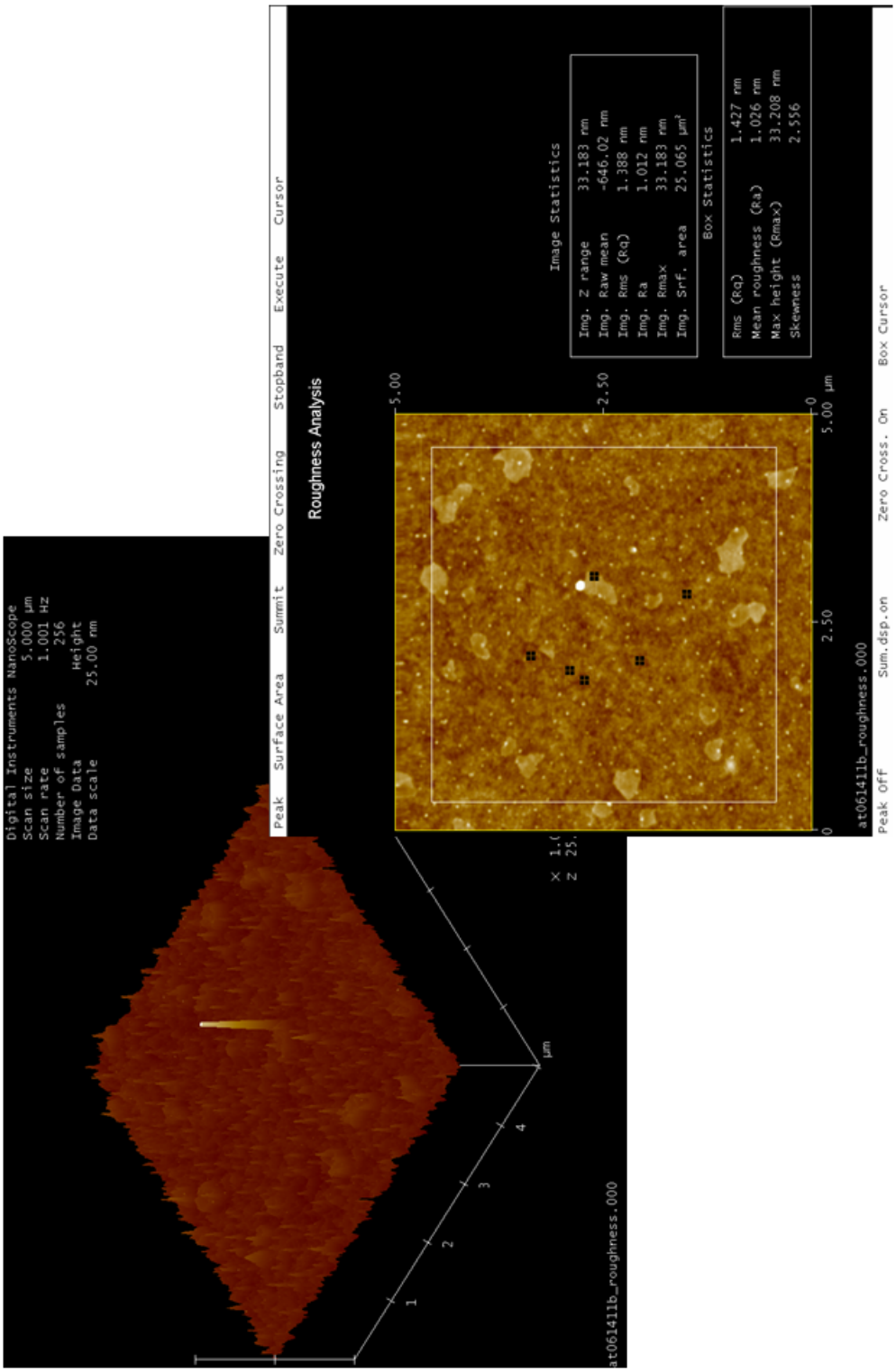

Figure 3.6 AFM Surface Roughness Micrograph of a Spin-Coated Organic Bulk Heterojunction Solar Cell

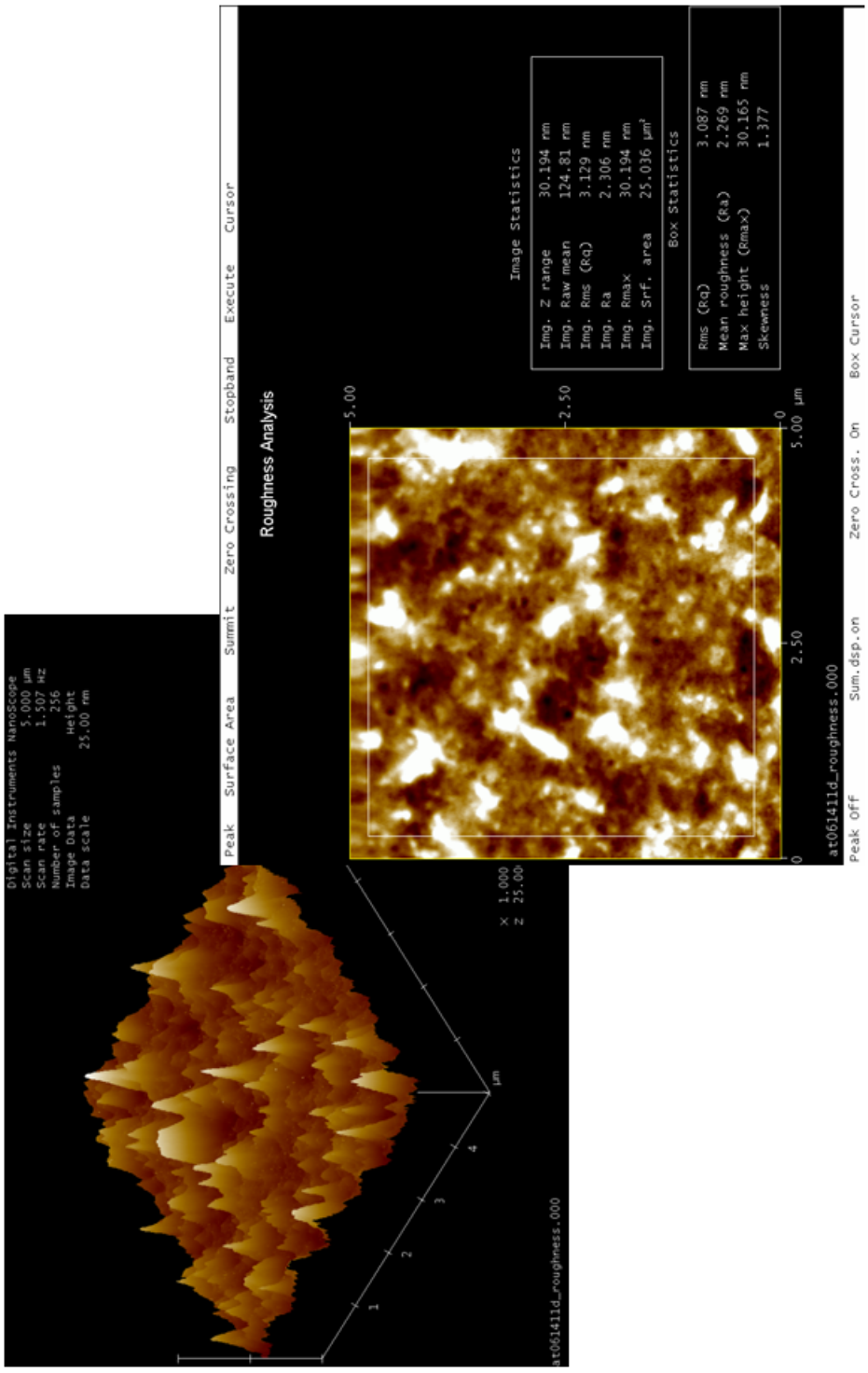

Figure 3.7 AFM Surface Roughness of a Paint-Brushed Organic Bulk Heterojunction Solar Cell

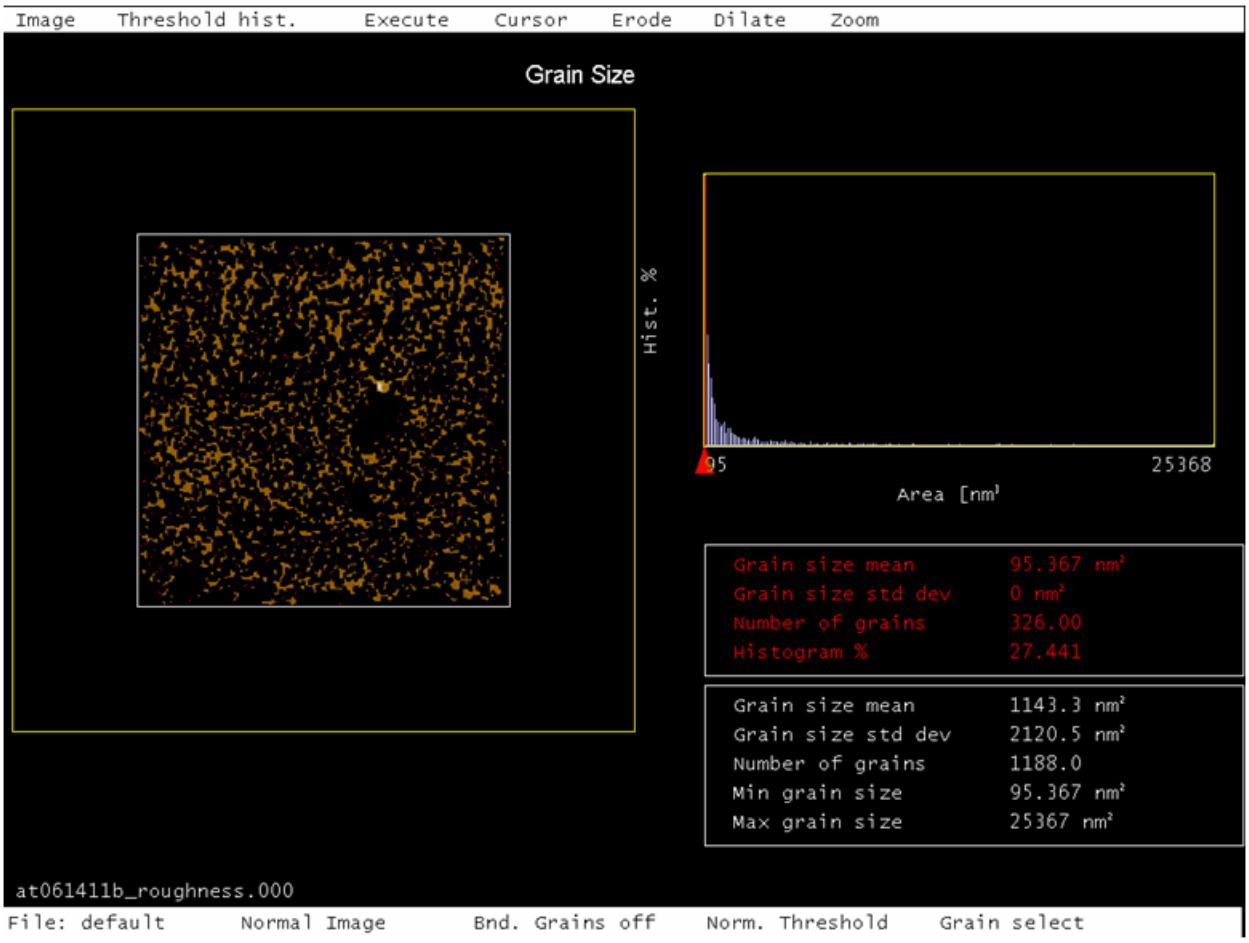

Figure 3.8 AFM Phase Micrograph of a Spin-Coated Organic Bulk Heterojunction Solar Cell

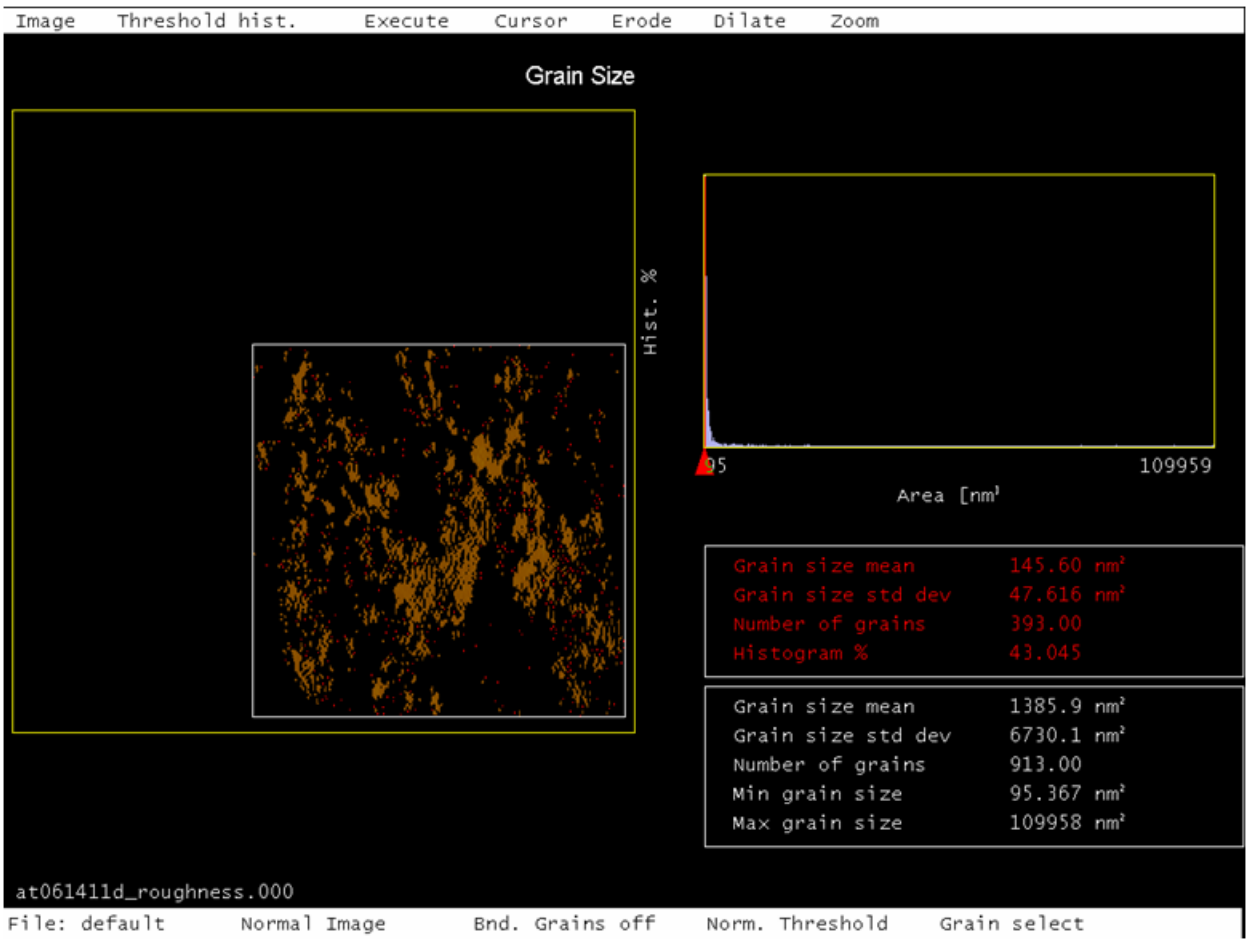

Figure 3.9 AFM Phase Micrograph of a Paint-Brushed Organic Bulk Heterojunction Solar Cell

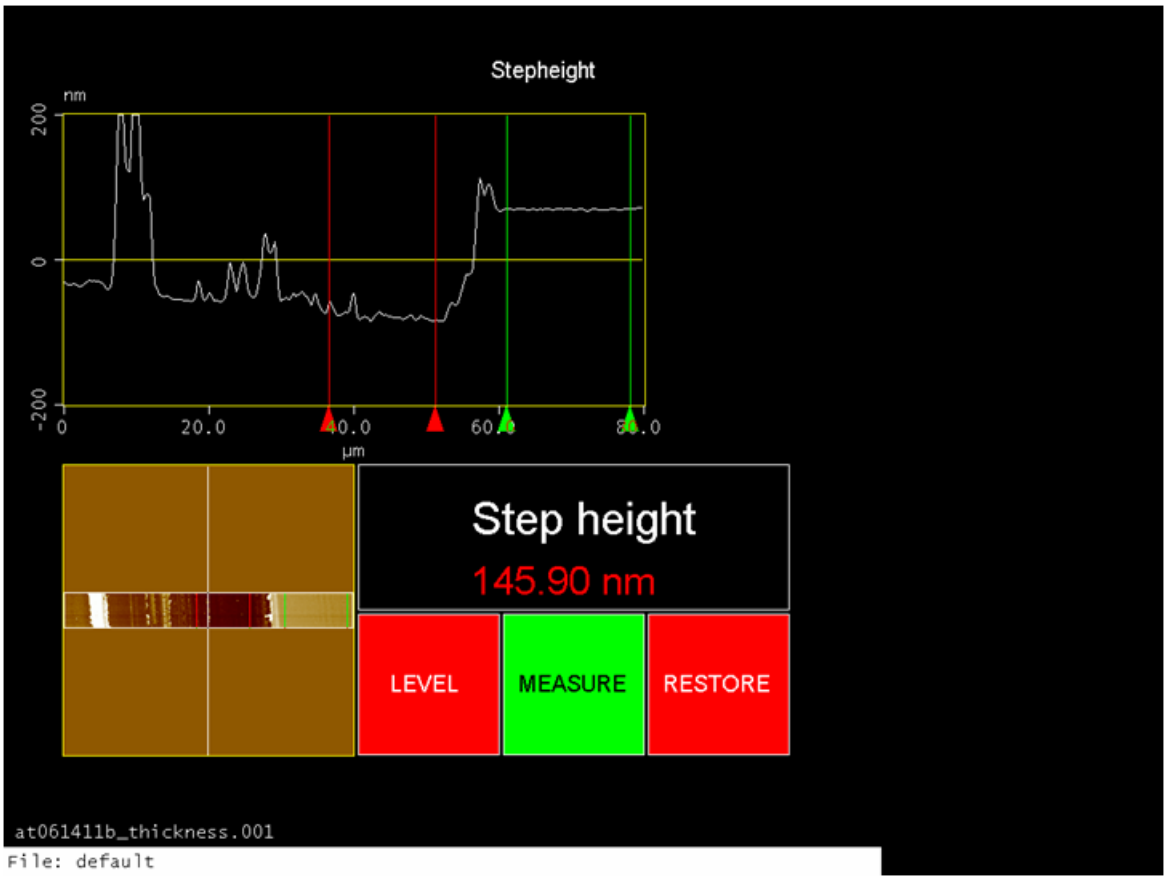

Figure 3.10 AFM Thickness Micrograph of a Spin-Coated Organic Bulk Heterojunction Solar Cell

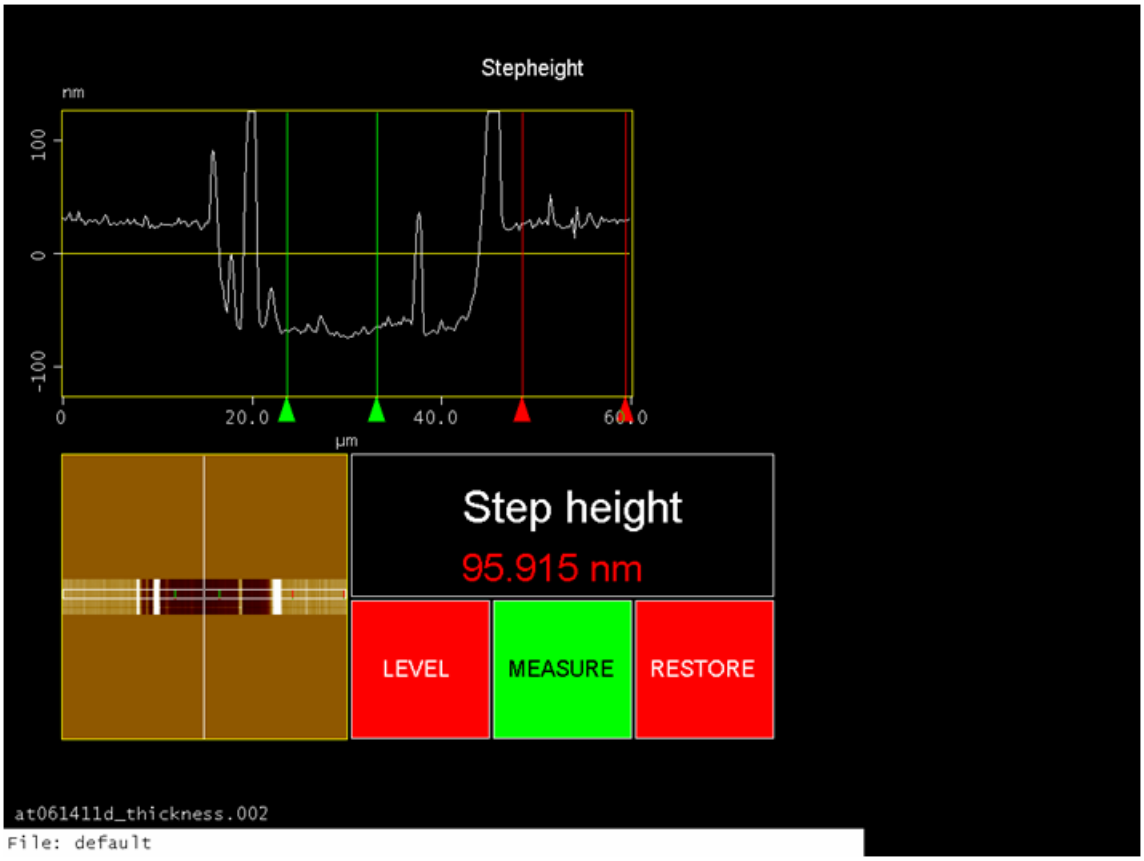

Figure 3.11 AFM Thickness Micrograph of a Paint-Brushed Organic Bulk Heterojunction Solar Cell

CHAPTER 4. CONCLUSION

4.1 Future Work

This section of this academic work covers possible future work related to the paintbrush deposition technique for the fabrication of organic bulk heterojunction solar cells. Additional device characterization techniques will be described in an effort to encourage further study of organic bulk heterojunction solar cell devices fabricated by means of the paintbrush deposition technique. Fabrication studies in which the effects of altering fabrication parameters are studied will also be suggested to further expand the knowledge pertaining to this organic solar cell fabrication technique. Lastly, this section will cover photoluminescence-based oxygen and biochemical sensing utilizing organic electronics, a promising application for organic bulk heterojunction solar cell devices fabricated by means of the paintbrush deposition technique. Results from studies on utilizing paint-brushed organic bulk heterojunction solar cells for photoluminescent oxygen sensing will be presented and discussed.

4.1.1 Further Research into the Paintbrush Deposition Technique

The research presented in this academic work does not by any means constitute a fully comprehensive study of the paintbrush deposition technique for solution processing organic electronic devices. The findings reported here only pertain to using the paintbrush deposition technique in solution processing P3HT:PCBM organic semiconducting systems from chlorobenzene solutions. First and foremost, further research into the paintbrush deposition technique should be catered towards improving the power conversion efficiencies of organic solar cell devices fabricated with this solution processing technique. Also, reducing or eradicating the excessive PCBM agglomeration within the paint-brushed active layer films should be a priority

to ensure that the paintbrush deposition technique can be adaptable to large scale industrial roll-to-roll fabrication processes. Altering the solution concentrations of P3HT and PCBM may help with increasing power conversion efficiencies and decreasing the excessive PCBM agglomeration. Also, using different solution solvents, and perhaps stronger solvents for PCBM than chlorobenzene, may decrease the excessive PCBM agglomeration in the active layer films of the paint-brushed devices. Altering the polymer and fullerene concentrations and solution solvents will also alter the nano-scale morphology of the active layer films, providing more areas of research dealing with the paintbrush deposition technique. Further studies into the paintbrush deposition technique could and should involve utilizing different semiconducting organic materials, such as low band-gap semiconducting polymers.

In addition to the measurements conducted in this research study on the paintbrush deposition technique, more research techniques and measurements may be used to further expand the knowledge pertaining to this novel solution processing technique for fabricating organic solar cell devices. Space charge limited current measurements could provide hole mobility data within the bulk heterojunction active layers of organic solar cell devices fabricated by the paintbrush deposition technique. Trap measurements utilizing small signal capacitive models could also provide information on the operation of organic solar cell devices fabricated by using the paintbrush deposition technique. Micrographs of active layer films of organic solar cell devices fabricated by the paintbrush deposition technique provided by scanning electron microscopes or transmission electron microscopes can also provide information on the resulting nano-scale morphologies of the resulting bulk heterojunctions created by this fabrication technique.

4.1.2 Application to Oxygen and Biochemical Sensing

The paintbrush deposition technique obviously has potential to be a simple solution processing technique for applying organic semiconducting active layers upon substrates in a large industrial roll-to-roll fabrication process. However, the paintbrush deposition technique can be useful for small scale laboratory work with unique requirements impeding the use of more traditional methods for solution processing organic semiconductor materials. One example of a unique small scale laboratory requirement for the paintbrush deposition technique is the

fabrication of photoluminescence-based organic oxygen and biochemical sensors. In 2010, Nalwa et al. reported on photoluminescence-based oxygen and biochemical sensors utilizing organic photodiodes based on the P3HT:PCBM donor/acceptor semiconducting system [50]. The photoluminescence-based oxygen and biochemical sensors reported by Nalwa et al. are comprised of a green light-emitting-diode as an excitation source, an oxygen and biochemical sensitive photoluminescent dye, and an organic photodetector. Figure 4.1 depicts the photoluminescence-based oxygen and biochemical sensor architecture that Nalwa et al. employed and reported in their 2010 study.

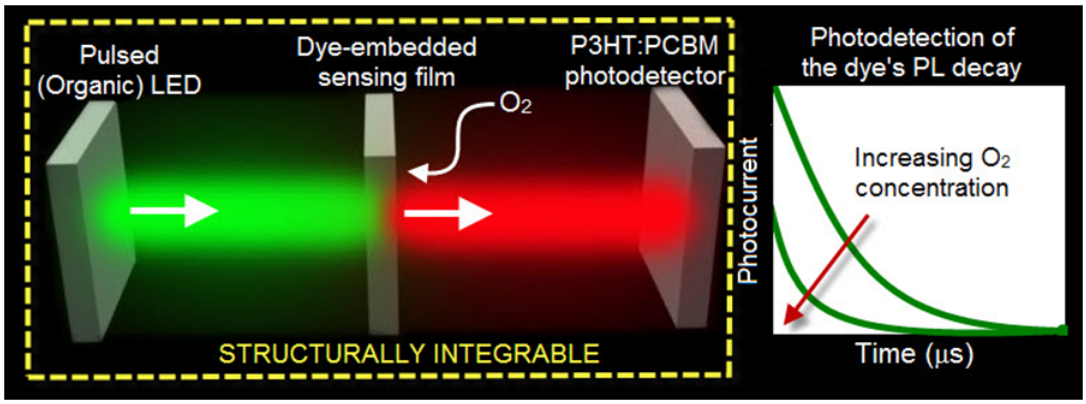

Figure 4.1 A Photoluminescence-based Non-integrated Oxygen Sensor

In order to sense oxygen, the sensors with the architecture in Figure 4.1 operate by exciting an oxygen sensitive photoluminescent dye with a green light-emitting-diode. The oxygen-sensitive dye emits red light upon excitation by the green light emitted from the green light-emitting diode, the amount of which is dependent upon the concentration of oxygen surrounding the dye, which in turn is detected by the organic photodetector. Lower intensities of red light detected by the organic photodetector correspond to higher concentrations of oxygen surrounding the dye. If the green light-emitting-diode is pulsed, then the time constants of the photodetection decay between the green light pulses can also be used to determine the oxygen concentration surrounding the dye, with lower time constants indicating higher concentrations of oxygen. An illustration of typical photodetection decay curves measured by the organic photodetectors in the photoluminescence-based oxygen sensors reported by Nalwa et al. can be found in Figure 4.1. The oxygen-sensitive dye used in the sensors reported by Nalwa et al.

was platinum octaethylporphyrin (PtOEP) embedded in a titanium oxide doped polystyrene film[50]. The collisions of the surrounding oxygen atoms with the oxygen sensitive dye result in the the photoluminescence quenching of red light emitted from the oxygen sensitive dye in the sensors reported by Nalwa et al. providing the mechanism by which the concentration of oxygen surrounding the dye can be determined. Nalwa et al. also reported that glucose sensing could be achieved with the same photoluminescent-based sensing architecture used for oxygen sensing[50].

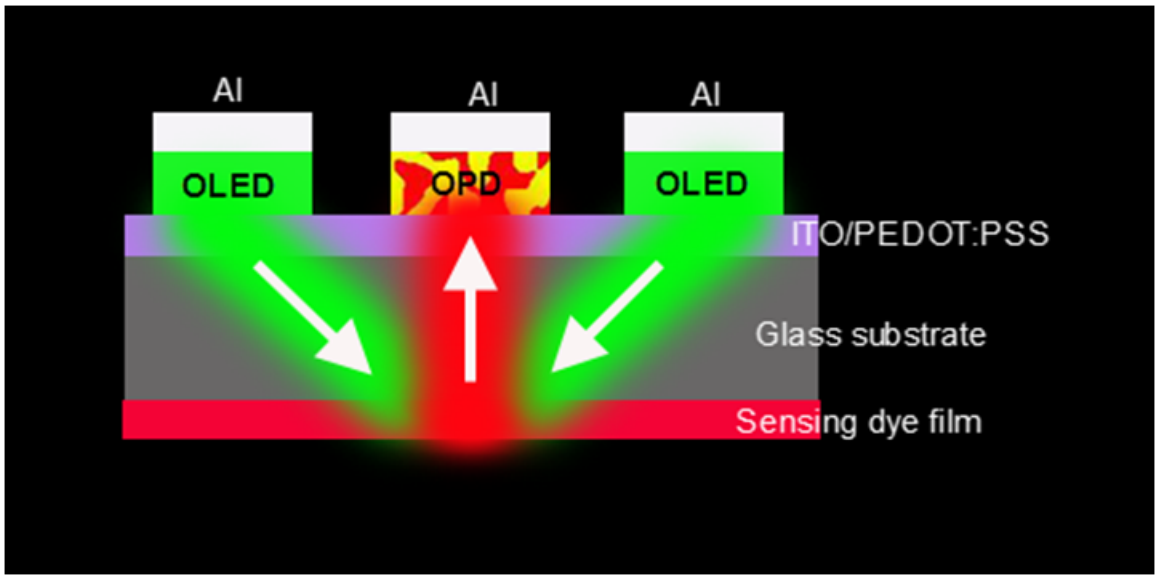

Figure 4.2 A Completely Integrated Organic Photoluminescent-based Oxygen Sensor

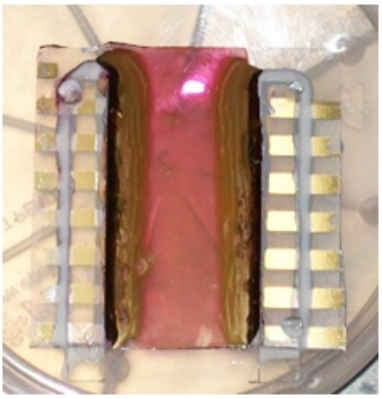

Figure 4.3 A Partially Fabricated Integrated Organic Photoluminescence-based Oxygen Sensor

The results reported by Nalwa et al. in their 2010 study of non-integrated photoluminescence-based oxygen and biochemical sensors showed great promise for oxygen and biochemical sensing using organic electronic components. However, an integrated photoluminescence-based oxygen and biochemical sensing architecture is desirable for progressing photoluminescence-based oxygen and biochemical sensing using organic electronics from laboratory research to being part of a usable product. Figure 4.2 depicts an integrated photoluminescence-based oxygen and biochemical sensor comprised of only organic-based electronics. As can be seen from Figure 4.2, the paintbrush deposition technique would be ideal for fabricating the organic photodetector in a precise, controlled manner for this integrated sensing architecture. Another benefit to fabricating the photodetector in the integrated oxygen and biochemical sensor shown in Figure 4.2 by means of the paintbrush deposition technique is that the resulting photodetector will have decent red photon detection, a critical requirement for oxygen and biochemical sensing, as discussed in Section 3.3 and Section 3.4. Preliminary studies involving the fabrication and testing of organic integrated photoluminescence-based oxygen and biochemical sensors have been conducted without netting successful results. Fabricating such integrated sensors is difficult and time consuming due to requiring the use of different fabrication methods such as small molecule evaporation, drop-casting, paint-brushing, and the thermal evaporation of metal. Also, more optical engineering may be required than what is suggested by the organic integrated sensor depicted in Figure 4.2 in order for this integrated sensing architecture to work. Figure 4.3 shows a picture of a partially fabricated organic integrated circuit based on the architecture presented in Figure 4.2.

Despite the difficulties found with fabricating and testing organic integrated photoluminescence-based oxygen and biochemical sensors, success has been found with testing semi-integrated sensors. Figure 4.4 depicts the architecture of a semi-integrated photoluminescence-based oxygen and biochemical sensor architecture. In the semi-integrated sensor architecture the oxygen and biochemical sensitive dye and organic photodetector are fabricated on the same glass slide substrate. The semi-integrated photoluminescence-based oxygen and biochemical sensor architecture does not integrate the green light-emitting-diodes, sacrificing device integration for ease of fabrication and engineering. Figure 4.4 shows actual measured curves of photolumi-

nescence intensity decay detected by the organic photodetector from the excited sensing dye for laboratory fabricated semi-integrated oxygen sensors. Given the success of utilizing the paintbrush deposition technique for fabricating organic photodetectors used in non-integrated and semi-integrated photoluminescence-based oxygen and biochemical sensors, the paintbrush deposition technique holds great promise in bringing forth the realization of fully integrated organic photoluminescence-based oxygen and biochemical sensors.

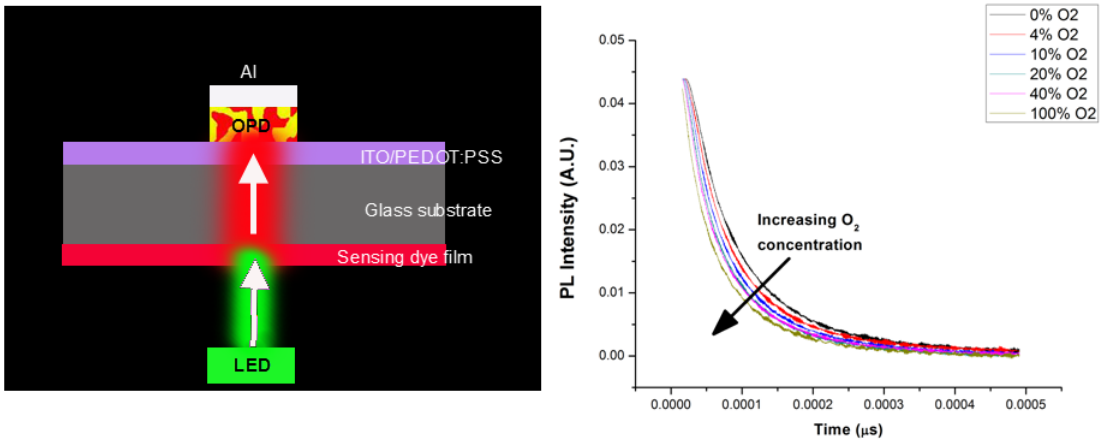

Figure 4.4 A Semi-integrated Photoluminescence-based Oxygen Sensor

4.2 Research Summary

This academic study focused on the paintbrush deposition fabrication technique for organic bulk heterojunction solar cell devices, a novel solution processing technique with a promising future. In this study, organic bulk heterojunction solar cell devices based on the P3HT:PCBM donor/acceptor polymer and fullerene organic semiconducting system were fabricated, in part, by solution processing involving white nylon paintbrushes. For comparison purposes, the active layers of the organic bulk heterojunction solar cells were deposited by paint-brushing and the more traditional solution processing technique, spin-coating. Both paint-brushed and spin-coated organic solar cells shared the same organic solar cell architecture incorporating: an indium-tin-oxide sputtered glass substrate, a PEDOT:PSS transparent buffer layer, a P3HT:PCBM bulk heterojunction active layer, and an aluminum top metal electrode layer.

The paint-brushed and spin-coated organic solar cell device evaluated in this study were fabricated under the same circumstances in order for direct comparisons of the different fabrication techniques to be made.

Many characterization techniques were used to study the device performance of organic bulk heterojunction solar cell devices fabricated by means of the paint brush deposition technique. For device performance comparison purposes, those same characterization techniques were also applied to organic bulk heterojunction solar cell devices fabricated by spin-coating. The characterization techniques employed for studying the device performance of the paint-brushed and spin-coated organic solar cells in this study included: measuring light current-voltage characteristics, measuring dark current-voltage characteristics, measuring the absorbance of the active layer films, and measuring normalized relative external quantum efficiencies. Atomic force microscopy was utilized to produce topography and phase micrographs for active layer films created by paint-brushing and spin-coating. Atomic force microscopy was also utilized to determine the thicknesses of the active layer films in the paint-brushed and spin-coated organic solar cells in this study.

The characterization techniques and measurements described above showed a fundamental difference in performance between devices fabricated by the paintbrush deposition technique and the more traditional spin-coating deposition technique. Light current-voltage measurements showed a nearly doubled power conversion efficiency increase of the the paint-brushed organic solar cell devices over the spin-coated devices. The light light-current voltage measurements also showed that the spin-coated devices had an S-shaped current-voltage characteristic, which is indicative of a potential barrier impeding charge collection within a solar cell device. This potential barrier was ascribed to be due to a lack of PCBM acceptor molecules at the metal cathode interface, most likely as a result from the quicker drying times of the solution processed active layers of the spin-coated organic solar cell devices with respect to those of the paint-brushed devices. Dark current-voltage measurements corroborated the findings from the light current voltage measurements by showing that the spin-coated devices had poor electron injection from the metal cathode, resulting in dark current-voltage measurements that were a couple magnitudes lower than measurements from paint-brushed devices. Absorbance

measurements also showed a stark contrast in performance between paint-brushed and spin-coated organic solar cells. The absorbance measurements of the paint-brushed devices showed an absorbance spectrum with three distinct vibronic peaks and more red photon absorbance in comparison to the absorbance spectrum from the spin-coated devices, both of which are indicative of a more crystalline polymer phase with enhanced conjugation. External quantum efficiency measurements showed that the paint-brushed devices collected more charge carriers from red photons than the spin-coated devices, which is due to the enhanced absorbance in the red region of the solar spectrum for the paint-brushed devices. Surface topography, phase, and thickness micrographs were obtained via atomic force microscopy in order to analyze both paint-brushed and spin-coated devices. Surface topography micrographs showed that paint-brushed devices had rougher surfaces than those from spin-coated devices, most likely due to more PCBM agglomeration at the surface of the active layer films in paint-brushed devices. Phase micrographs showed that there were larger grains within the paint-brushed samples than within the spin-coated samples, which is likely due to the increased polymer conjugation and PCBM agglomeration in paint-brushed samples as a result of the relatively slower active layer drying times. Thickness micrographs showed that the paint-brushed devices were slightly thinner than the spin-coated devices, which shows that the increased red absorbance within the paint-brushed devices was not due to a thicker active layer in the paint-brushed devices.

This study of the paintbrush deposition technique for solution processing organic bulk heterojunction solar cell devices showed that for organic solar cells based on the P3HT:PCBM donor/acceptor polymer and fullerene organic semiconducting system and with active layers solution processed from chlorobenzene solution that paint-brushed organic solar cells perform better than spin-coated organic solar cells. The key to the paintbrush deposition technique appears to be the slower drying times for the active layers of paint-brushed devices that allow a more favorable nano-scale morphology to be established without undesirable vertical phase separation of the PCBM acceptor molecules. The paintbrush deposition technique produces devices that show greater red light detection over spin-coated solar cell devices for organic solar cells solution processed from chlorobenzene solution. This enhanced red light detection may prove useful for harvesting more of the solar energy spectrum incident upon the Earth or for niche

applications specifically requiring enhanced red light detection, such as in photoluminescence-based oxygen and biochemical sensing. The paintbrush deposition technique does currently have issues that need to be resolved in order for it to be a productive fabrication technique. The excessive PCBM agglomeration found in paint-brushed organic solar cells needs to be eradicated or minimized in order for a greater usable area for fabricated paint-brushed organic solar cell devices to be obtained. Power conversion efficiencies also need to be increased in devices fabricated from the paintbrush deposition technique in order for the solution processing technique to be competitive with more traditional solution processing techniques being utilized in the organic semiconducting research field and industry. Despite these issues, the paintbrush deposition technique holds promise as an efficient and simple organic photovoltaics solution processing technique applicable to both large industrial roll-to-roll processing operations and small research laboratory operations.

BIBLIOGRAPHY

[1] S. Günes, H. Neugebauer, and N. S. Sariciftci, "Conjugated Polymer-Based organic solar cells," *Chemical Reviews*, vol. 107, pp. 1324–1338, Apr. 2007.

[2] D. E. Markov, E. Amsterdam, P. W. M. Blom, A. B. Sieval, and J. C. Hummelen, "Accurate measurement of the exciton diffusion length in a conjugated polymer using a heterostructure with a Side-Chain Cross-Linked fullerene layer," *The Journal of Physical Chemistry A*, vol. 109, pp. 5266–5274, June 2005.

[3] P. E. Shaw, A. Ruseckas, and I. D. W. Samuel, "Exciton diffusion measurements in poly(3-hexylthiophene)," *Advanced Materials*, vol. 20, pp. 3516–3520, Sept. 2008.

[4] P. W. Blom, V. D. Mihailetchi, L. J. Koster, and D. E. Markov, "Device physics of Polymer:Fullerene bulk heterojunction solar cells," *Advanced Materials*, vol. 19, pp. 1551–1566, June 2007.

[5] H. W. Kroto, J. R. Heath, S. C. O'Brien, R. F. Curl, and R. E. Smalley, "C60: Buckminsterfullerene," *Nature*, vol. 318, pp. 162–163, Nov. 1985.

[6] N. S. Sariciftci, L. Smilowitz, A. J. Heeger, and F. Wudl, "Photoinduced electron transfer from a conducting polymer to buckminsterfullerene," *Science*, vol. 258, pp. 1474 –1476, Nov. 1992.

[7] J. C. Hummelen, B. W. Knight, F. LePeq, F. Wudl, J. Yao, and C. L. Wilkins, "Preparation and characterization of fulleroid and methanofullerene derivatives," *The Journal of Organic Chemistry*, vol. 60, pp. 532–538, Feb. 1995.

[8] C. J. Brabec, N. S. Sariciftci, and J. C. Hummelen, "Plastic solar cells," *Advanced Functional Materials*, vol. 11, pp. 15–26, Feb. 2001.

[9] R. Partridge, "Electroluminescence from polyvinylcarbazole films: 1. carbazole cations," *Polymer*, vol. 24, pp. 733–738, June 1983.

[10] R. Partridge, "Electroluminescence from polyvinylcarbazole films: 2. polyvinylcarbazole films containing antimony pentachloride," *Polymer*, vol. 24, pp. 739–747, June 1983.

[11] R. Partridge, "Electroluminescence from polyvinylcarbazole films: 3. electroluminescent devices," *Polymer*, vol. 24, pp. 748–754, June 1983.

[12] R. Partridge, "Electroluminescence from polyvinylcarbazole films: 4. electroluminescence using higher work function cathodes," *Polymer*, vol. 24, pp. 755–762, June 1983.

[13] J. H. Burroughes, D. D. C. Bradley, A. R. Brown, R. N. Marks, K. Mackay, R. H. Friend, P. L. Burns, and A. B. Holmes, "Light-emitting diodes based on conjugated polymers," *Nature*, vol. 347, pp. 539–541, Oct. 1990.

[14] D. Braun and A. J. Heeger, "Visible light emission from semiconducting polymer diodes," *Applied Physics Letters*, vol. 58, no. 18, p. 1982, 1991.

[15] P. Schilinsky, C. Waldauf, J. Hauch, and C. J. Brabec, "Polymer photovoltaic detectors: progress and recent developments," *Thin Solid Films*, vol. 451-452, pp. 105–108, Mar. 2004.

[16] P. Peumans and S. R. Forrest, "Separation of geminate charge-pairs at donor-acceptor interfaces in disordered solids," *Chemical Physics Letters*, vol. 398, pp. 27–31, Nov. 2004.

[17] V. D. Mihailetchi, L. J. A. Koster, J. C. Hummelen, and P. W. M. Blom, "Photocurrent generation in Polymer-Fullerene bulk heterojunctions," *Physical Review Letters*, vol. 93, p. 216601, Nov. 2004.

[18] C. W. Tang, "Two-layer organic photovoltaic cell," *Applied Physics Letters*, vol. 48, no. 2, p. 183, 1986.

[19] N. S. Sariciftci, D. Braun, C. Zhang, V. I. Srdanov, A. J. Heeger, G. Stucky, and F. Wudl, "Semiconducting polymer-buckminsterfullerene heterojunctions: Diodes, photodiodes, and photovoltaic cells," *Applied Physics Letters*, vol. 62, no. 6, p. 585, 1993.

[20] J. J. M. Halls, K. Pichler, R. H. Friend, S. C. Moratti, and A. B. Holmes, "Exciton diffusion and dissociation in a poly(p-phenylenevinylene)/C60 heterojunction photovoltaic cell," *Applied Physics Letters*, vol. 68, no. 22, p. 3120, 1996.

[21] K. Tada, M. Onoda, and A. A. Zakhidov, "Characteristics of poly(p-pyridyl vinylene)/Poly(3-alkylthiophene) heterojunction photocell," *Japanese Journal of Applied Physics*, vol. 36, pp. L306–L309, Mar. 1997.

[22] S. A. Jenekhe and S. Yi, "Efficient photovoltaic cells from semiconducting polymer heterojunctions," *Applied Physics Letters*, vol. 77, no. 17, p. 2635, 2000.

[23] K. H. Lee, P. E. Schwenn, A. R. G. Smith, H. Cavaye, P. E. Shaw, M. James, K. B. Krueger, I. R. Gentle, P. Meredith, and P. L. Burn, "Morphology of All-Solution-Processed Bilayer organic solar cells," *Advanced Materials*, vol. 23, pp. 766–770, Feb. 2011.

[24] G. Yu, J. Gao, J. C. Hummelen, F. Wudl, and A. J. Heeger, "Polymer photovoltaic cells: Enhanced efficiencies via a network of internal Donor-Acceptor heterojunctions," *Science*, vol. 270, pp. 1789 –1791, Dec. 1995.

[25] S. E. Shaheen, C. J. Brabec, N. S. Sariciftci, F. Padinger, T. Fromherz, and J. C. Hummelen, "2.5% efficient organic plastic solar cells," *Applied Physics Letters*, vol. 78, no. 6, p. 841, 2001.

[26] W. Ma, C. Yang, X. Gong, K. Lee, and A. J. Heeger, "Thermally stable, efficient polymer solar cells with nanoscale control of the interpenetrating network morphology," *Advanced Functional Materials*, vol. 15, pp. 1617–1622, Oct. 2005.

[27] G. Li, V. Shrotriya, J. Huang, Y. Yao, T. Moriarty, K. Emery, and Y. Yang, "High-efficiency solution processable polymer photovoltaic cells by self-organization of polymer blends," *Nat Mater*, vol. 4, pp. 864–868, Nov. 2005.

[28] C. J. Brabec, A. Cravino, D. Meissner, N. S. Sariciftci, T. Fromherz, M. T. Rispens, L. Sanchez, and J. C. Hummelen, "Origin of the open circuit voltage of plastic solar cells," *Advanced Functional Materials*, vol. 11, pp. 374–380, Oct. 2001.

[29] S. H. Park, A. Roy, S. Beaupre, S. Cho, N. Coates, J. S. Moon, D. Moses, M. Leclerc, K. Lee, and A. J. Heeger, "Bulk heterojunction solar cells with internal quantum efficiency approaching 100%," *Nat Photon*, vol. 3, pp. 297–302, May 2009.

[30] H. Chen, J. Hou, S. Zhang, Y. Liang, G. Yang, Y. Yang, L. Yu, Y. Wu, and G. Li, "Polymer solar cells with enhanced open-circuit voltage and efficiency," *Nat Photon*, vol. 3, pp. 649–653, Nov. 2009.

[31] Y. Liang, Z. Xu, J. Xia, S. Tsai, Y. Wu, G. Li, C. Ray, and L. Yu, "For the bright Future-Bulk heterojunction polymer solar cells with power conversion efficiency of 7.4%," *Advanced Materials*, vol. 22, pp. E135–E138, May 2010.

[32] L. J. A. Koster, V. D. Mihailetchi, and P. W. M. Blom, "Ultimate efficiency of polymer/fullerene bulk heterojunction solar cells," *Applied Physics Letters*, vol. 88, no. 9, p. 093511, 2006.

[33] B. Walker, A. B. Tamayo, X. Dang, P. Zalar, J. H. Seo, A. Garcia, M. Tantiwiwat, and T. Nguyen, "Nanoscale phase separation and high photovoltaic efficiency in Solution-Processed, Small-Molecule bulk heterojunction solar cells," *Advanced Functional Materials*, vol. 19, pp. 3063–3069, Oct. 2009.

[34] J. J. M. Halls, C. A. Walsh, N. C. Greenham, E. A. Marseglia, R. H. Friend, S. C. Moratti, and A. B. Holmes, "Efficient photodiodes from interpenetrating polymer networks," *Nature*, vol. 376, no. 6540, pp. 498–500, 1995.

[35] M. M. Koetse, J. Sweelssen, K. T. Hoekerd, H. F. M. Schoo, S. C. Veenstra, J. M. Kroon, X. Yang, and J. Loos, "Efficient polymer:polymer bulk heterojunction solar cells," *Applied Physics Letters*, vol. 88, no. 8, p. 083504, 2006.

[36] W. Shockley and H. J. Queisser, "Detailed balance limit of efficiency of p-n junction solar cells," *Journal of Applied Physics*, vol. 32, no. 3, p. 510, 1961.

[37] A. D. Vos, "Detailed balance limit of the efficiency of tandem solar cells," *Journal of Physics D: Applied Physics*, vol. 13, pp. 839–846, May 1980.

[38] T. Ameri, G. Dennler, C. Lungenschmied, and C. J. Brabec, "Organic tandem solar cells: A review," *Energy & Environmental Science*, vol. 2, no. 4, p. 347, 2009.

[39] J. Y. Kim, K. Lee, N. E. Coates, D. Moses, T. Nguyen, M. Dante, and A. J. Heeger, "Efficient tandem polymer solar cells fabricated by All-Solution processing," *Science*, vol. 317, pp. 222 –225, July 2007.

[40] J. D. Kotlarski and P. W. M. Blom, "Ultimate performance of polymer:fullerene bulk heterojunction tandem solar cells," *Applied Physics Letters*, vol. 98, no. 5, p. 053301, 2011.

[41] G. Dennler, M. C. Scharber, T. Ameri, P. Denk, K. Forberich, C. Waldauf, and C. J. Brabec, "Design rules for donors in Bulk-Heterojunction tandem solar Cells-Towards 15% Energy-Conversion efficiency," *Advanced Materials*, vol. 20, pp. 579–583, Feb. 2008.

[42] F. C. Krebs, "Fabrication and processing of polymer solar cells: A review of printing and coating techniques," *Solar Energy Materials and Solar Cells*, vol. 93, pp. 394–412, Apr. 2009.

[43] M. R. Lee, R. D. Eckert, K. Forberich, G. Dennler, C. J. Brabec, and R. A. Gaudiana, "Solar power wires based on organic photovoltaic materials," *Science*, vol. 324, pp. 232 –235, Apr. 2009.

[44] J. W. Jung and W. H. Jo, "Annealing-Free high efficiency and large area polymer solar cells fabricated by a roller painting process," *Advanced Functional Materials*, vol. 20, pp. 2355–2363, July 2010.

[45] S. S. Kim, S. I. Na, J. Jo, G. Tae, and D. Y. Kim, "Efficient polymer solar cells fabricated by simple brush painting," *Advanced Materials*, vol. 19, pp. 4410–4415, Dec. 2007.

[46] S. Kim, S. Na, S. Kang, and D. Kim, "Annealing-free fabrication of P3HT:PCBM solar cells via simple brush painting," *Solar Energy Materials and Solar Cells*, vol. 94, pp. 171–175, Feb. 2010.

[47] J. Pallares, R. Cabre, L. F. Marsal, and R. E. I. Schropp, "A compact equivalent circuit for the dark current-voltage characteristics of nonideal solar cells," *Journal of Applied Physics*, vol. 100, no. 8, p. 084513, 2006.

[48] B. Tremolet de Villers, C. J. Tassone, S. H. Tolbert, and B. J. Schwartz, "Improving the reproducibility of P3HT:PCBM solar cells by controlling the PCBM/Cathode interface," *The Journal of Physical Chemistry C*, vol. 113, pp. 18978–18982, Nov. 2009.

[49] K. Vandewal, K. Tvingstedt, A. Gadisa, O. Inganas, and J. V. Manca, "On the origin of the open-circuit voltage of polymer-fullerene solar cells," *Nat Mater*, vol. 8, pp. 904–909, Nov. 2009.

[50] K. S. Nalwa, Y. Cai, A. L. Thoeming, J. Shinar, R. Shinar, and S. Chaudhary, "Polythiophene-Fullerene based photodetectors: Tuning of spectral response and application in photoluminescence based (Bio)Chemical sensors," *Advanced Materials*, vol. 22, pp. 4157–4161, Oct. 2010.